Utrecht University

Master Thesis

Kevin Daalhuizen

Nanoconfined Sodium Alanate as a Transition Metal Free Hydrogenation Catalyst

Supervisors:

P. Bramwell
Prof. P. E. de Jongh
Prof. R. J. M. Klein Gebbink

Inorganic Chemistry and Catalysis
Debye Institute for Nanomaterials Science
Utrecht University

Abstract

Nanoconfined sodium alanate was shown to be active as a transition metal free hydrogenation catalyst in the hydrogenation of diphenylacetylene. The catalyst was optimized in terms of preparation method, support material and catalyst loading. The best performing catalysts consisted of 20 weight percent of sodium alanate, melt infiltrated into carbon xerogel or high surface area graphite. These catalysts showed a diphenylacetylene conversion of 90% in 4 hours, at 190 ˚C under a 100 bar H_2 atmosphere. A substrate screening showed the catalyst to be active for other substrates containing carbon-carbon double bonds as well, however activity is higher for less substituted double bonds. Oxygen containing substrates were tested as well, but were found to deactivate the catalyst. To learn more about the catalytic mechanism, a deuterated catalyst was succesfully prepared by melt infiltration of sodium alanate under deuterium atmosphere. This catalyst was tested in deuterating of norbornene and with a combination of ^1H and ^2H NMR experiments it was shown that hydrogenation proceeds through syn-addition.

List of Abbreviations

Throughout this thesis different units and abbreviations will be used which are specified in the list below:

APT	*Attached proton test*
BB	*Bibenzyl*
CX-xx	*Carbon xerogel with an average pore diameter of xx nm*
DPA	*Diphenylacetylene*
GC	*Gas-chromatography*
FLP	*Frustrated Lewis pairs*
HSAG-xx	*High surface area graphite with a surface area of xx* m^2/g
ID	*Inner diameter (e.g. of a GC-column)*
IWI	*Incipient wetness impregnation*
MI	*Melt infiltration*
MS	*Mass spectrometry*
NMR	*Nuclear magnetic resonance*
NPG	*Non-porous graphite (KS-6)*
PSD	*Pore size distribution*
RF	*Resorcinol-formaldehyde*
SEM	*Scanning electron microscopy*
TPD	*Temperature programmed desorption*
TGA	*Thermogravimetric analysis*
THF	*Tetrahydrofuran*
XRD	*X-ray diffraction*

Contents

List of Figures

List of Tables

Chapter 1

Introduction

Catalytic hydrogenation of organic molecules is a large-scale industrial process that is used, for example, in the upgrading of oil products, synthesis of mass consumer goods, but also in fine chemicals and medicinal chemistry. Usually expensive catalyst materials are needed and sometimes catalyst regeneration requires harsh conditions raising operating costs even further. Recently researchers have discovered that relatively cheap light metal hydrides, and sodium alanate in particular, are capable of reversibly storing large quantities of hydrogen. The conditions at which hydrogen release and possibly hydrogen absorption can be effected might make for a new class of hydrogenation catalysts that do not need expensive transition metals or transition metal complexes to be active. In this research paper an in-depth study toward the catalytic activity of sodium alanate in the hydrogenation of organic molecules is reported.

1.1 Catalytic hydrogenation

For organic molecules to spontaneously react with molecular hydrogen, rather extreme conditions are required. Temperatures upwards of 500 °C, often in combination with hydrogen pressures well above 100 bar, are no exception and even then reactions proceed slowly or hardly at all.[1] These conditions are not only hazardous because of the enormous amounts of highly flammable hydrogen gas that are required, but operating under these conditions also requires a lot of energy, all adding up to the total expenses.

It is possible to perform hydrogenation reactions of organic molecules under much milder conditions. To achieve this, hydrogenation catalysts are added. When chosen correctly, the catalyst will not only make it possible to operate at lower temperatures and pressures, but will also ensure a higher conversion and selectivity. The most commonly used hydrogenation catalysts consist of (supported) platinum group noblemetals. These catalysts can achieve good conversions under mild conditions with loadings as low as 2-5%[2]. The major drawback of these catalysts however, is that due to element scarcity they are very expensive.[a] This drawback is only magnified by the high temperatures needed for catalyst regeneration and the loss of the active metal through leeching.[3]

[a] platinum price: 28-35 USD/gram, January 2016

1.2 frustrated Lewis pairs

The idea of a transition metal free hydrogenation catalyst is not exactly new. For the better part of a decade, frustrated lewis pairs (FLP's) have been known to activate molecular hydrogen and research towards catalytic applications has been done.[4] FLP catalysts consist of a Lewis acid (e.g. $-P(C_6H_2Me_3)_2$) and a Lewis base (e.g. $-B(C_6F_5)_2$) which are part of the same structure, but in a way that prevents them from recombining to a Lewis adduct, or in other words, forming a *sterically congested Lewis pair.*[5] These FLP's have the ability to reversibly bind and activate hydrogen, which makes them good candidates for hydrogenation reactions. The group of Stephan et al. showed that, indeed, FLP's can be used as hydrogenation catalysts, however they only reached decent conversions when the substrate molecule contained electronegative groups like imines, nitriles or silyl enol ethers. For hydrogenation of, for example, ketones, aldehydes or olefins, FLP's seem less suitable. Even though addition to alkenes to form the zwitterionic product has been observed, hydrogenation is not observed at any noticeable rate.

1.3 Sodium alanate

Sodium alanate, or sodium aluminium hydride ($NaAlH_4$) is a white, pyrophoric powder that belongs to the complex metal hydride family and was first discovered in the late 1940's.[6] It has been used as a reducing agent in organic chemistry, but always in stoichiometric amounts.[7] More recently sodium alanate has become a popular candidate for reversible hydrogen storage. It contains 7.5 wt.% of hydrogen by weight, two thirds of which can theoretically be released by heating to 200 °C (Figure 1.1). Sodium alanate is of particular interest for applications requiring hydrogen cycling, because of its relatively high hydrogen content and its favourable enthalpy of hydrogen release, amounting to 37 kJ/mol H_2 and 47kJ/mol H_2 for the first two steps.[8]

$$\mathbf{3\,NaAlH_4(s) \longrightarrow Na_3AlH_6\,(s) + 2\,Al\,(s) + 3\,H_2\,(g) \quad 3.70\,wt\%\,H_2 \quad 37\ kJ/mol}$$

$$\mathbf{Na_3AlH_6(s) \longrightarrow 3\,NaH\,(s) + Al\,(s) + 1\,\tfrac{1}{2}\,H_2\,(g) \quad 1.85\,wt\%\,H_2 \quad 47\ kJ/mol}$$

$$\mathbf{NaH\,(s) \longrightarrow Na\,(l) + \tfrac{1}{2}\,H_2\,(g) \quad 1.85\,wt\%\,H_2 \quad at\ 400°C}$$

Figure 1.1 – *the complete 3-step dehydrogenation reaction of sodium alanate including the required temperature for each step for a 1 bar hydrogen equilibrium pressure. For full decomposition a temperature of 400 °C are needed for the consecutive steps to release 7.5 wt% hydrogen.*[9]

While bulk sodium alanate can only be dehydrogenated, its de/re- hydrogenation properties improve considerably when nanoconfined in a carbon matrix, reversibly releasing up to 5.5 wt% of hydrogen with respect to $NaAlH_4$ under mild conditions[10] and showing a hydrogen capacity retention over 80% after 15 de/re-hydrogenation cycles at 170 °C and 150 bars of pressure.[11]

By choosing the reaction conditions as to meet the requirements for both de- and re-hydrogenation it might be possible to use a sodium alanate catalyst for prolonged amounts of time, as it can cycle between the hydrogenated and (partially) dehydrogenated states without the need of a separate catalyst recycling step.

1.4 Nanoconfinement

During the last decade a lot of research has been done towards nano-sizing complex metal hydrides. Where the bulk materials often can only be dehydrogenated, nanoparticles, and especially supported nanoparticles, of the same material show immense improvements in hydrogen desorption, hydrogen resorption and cycling, all under relatively mild conditions.[12] While the decrease in crystalite size can be used as a partial explanation for several of these observations, for example because of reduced hydrogen diffusion pathlengths, the role of the support in these enhanced kinetics is not yet fully understood. It is thought to be a combination of support contributions that can be divided in electronic, structural and interface related effects.[13;14] An attempt at finding out more about the interactions between the carbon and sodium alanate by Verkuijlen et al. hinted at close contact between the different compounds and possibly a form of charge transfer effects, but the exact form of sodium remains unknown.[15] Another method that will not be further discussed in this thesis, but seems to enhance the hydrogen cycling kinetics of (nanoconfined) sodium alanate even further is doping with d-block metal catalysts like iron or titanium.[16] This is expected to be caused by Na-vacancies or defects in the sodium alanate crystal lattice, causing vacancy mediated hydrogen transport through the material.[17] This is the same effect that might improve hydrogen cycling upon nanoconfinement: when the pores are small enough the unit cells have to contain defects to fit inside.

1.4.1 Ball milling

Ball-milling is a commonly used method to prepare nanosized sodium alanate, or other light metal hydrides, in the presence of carbon or other support materials.[18;19] It is an easy and straightforward technique that allows for very high loadings of up to 90%, while maintaining a large positive effect on hydrogen cycling kinetics.[20] It also allows for the easy incorporation of kinetics enhancing dopants like titanium, e.g. in the form of $TiCl_4$.

Even though this method has been proven to work for hydrogen storage applications, it is probably not suitable for preparing hydrogenation catalysts. This is for multiple reasons. First of all, while the sodium alanate crystallite size is decreased to the nanoscale, the particle size distribution is broad and particles smaller than ∼150 nm are difficult to obtain.[21] Secondly, while the introduction of carbon seems to improve (de-)hydrogenation kinetics, the sodium alanate is not properly embedded inside the pores as is apparent from the possibility to reach loadings of 90%. This means that the active phase could be washed away during a catalysis reaction when a solvent is introduced.

Finally, ball-milled sodium alanate suffers from phase segregation, meaning Na and Al may no longer be in close contact, possibly reducing the reversible capacity. For this reason and because other convenient methods are available, ball milling will not be used in this research.

1.4.2 Melt infiltration

Preparing nanoconfined particles can be done by infiltration. In this process the sodium alanate is heated to temperatures exceeding its melting point in the presence of a porous support material, allowing capillary forces to fill the pores. Additionally, an overpressure of hydrogen is used, to prevent the decomposition of $NaAlH_4$ to Na_3AlH_6 or even NaH before the melting point is reached.

Melt infiltration is a relatively easy way to obtain high $NaAlH_4$/carbon loadings, provided that the support is chosen with care, since support wetting is the most limiting factor in terms of maximum loadings.[22] Loadings up to 30 wt% $NaAlH_4$ on carbon have been reported, for which the carbon pore structure is not changed compared to the pristine support and the metal hydride is only located inside carbon pores.[23] Higher loadings are possible, but not all of the sodium alanate will enter the pore system and some bulk behaviour can be seen.[14;24]

1.4.3 Incipient wetness impregnation

Since sodium alanate can be dissolved in THF, it is also possible to use impregnation techniques for the introduction of sodium alanate in carbon pores. Incipient wetness impregnation, or pore volume impregnation, makes it possible to decrease the sodium alanate particle size to the sub 10 nm range and increase the dispersion and therefore improve the kinetics of hydrogen desorption.[25] It is, however, a sensitive and complicated method with multiple challenges for the preparation of a $NaAlH_4$/carbon catalyst. To reach loadings comparable to melt infiltration, multiple impregnation steps are needed. For a sodium alanate loading of 20 wt% 5 impregnation/drying cycles were reported.[26] Drying is needed to remove any THF left in the pores and can best be done at low temperatures, to increase the solvent viscosity and therefore minimize the agglomeration of sodium alanate. Even though this is a rather straight-forward impregnation method, a side note has to be made. THF is known to complex with $LiAlH_4$[27] and will most likely show the same behaviour for sodium alanate. It is unknown how this complex will affect the impregnation procedure, but it is not unlikely the catalyst activity will be influenced.

1.5 Support materials

When nanoconfining light metal hydrides, the support has to be chosen with care. Since light metal hydrides tend to irreversibly react with certain oxygen containing groups, the ideal support material contains a small concentration of oxygen groups to provide nucleation sites for the active phase, without irreversibly oxidizing the entire active phase. Because of these restrictions carbon supports are often used when nanoconfining light metal hydrides, since their surface chemistry is well known and relatively easy to control, however, cases using a mesoporous silica support have also been reported.[26] In this study, carbon has been chosen as the support material, because it is both light and inert. Different carbon supports were prepared the characteristics of which will be further explained in sections 1.5.1 through 1.5.3. The reason for testing multiple supports is both to see whether a different pore size distribution (PSD) or morphology/crystallinity affects the catalyst and to be able to exclude or possibly investigate the role of carbon/sodium alanate interactions mentioned in section 1.4.

1.5.1 Carbon xerogel

Carbon xerogels are mesoporous carbon frameworks that can be used as catalyst support. They are prepared through a sol-gel condensation containing organic precursors, followed by drying and pyrolysis (Figure 1.2). They belong to the same type of compounds as aerogels and cryogels, which are dried under supercritical or cryogenic conditions respectively. Aero- and cryogels however, are even more porous than xerogels. Because xerogels are dried in air at a temperature of 90 °C, the surface tension of the water inside the pores is enough to make the gels partly collapse, creating mesoporous materials with a rather well defined pore size distribution.[28]

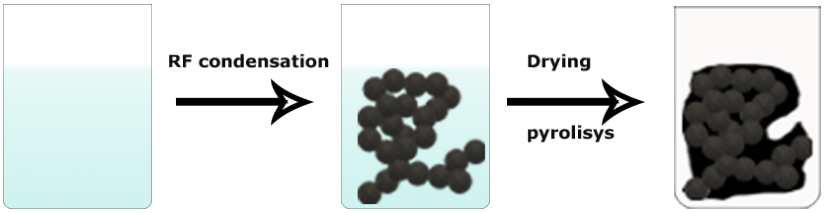

Figure 1.2 – *Different steps in carbon xerogel synthesis.*

Xerogels can be made from multiple materials, among which are silicon and carbon, but for this project only the carbon gels are relevant, because of their inert nature. The most common method to prepare xerogels found in literature is through a resorcinol-formaldehyde (RF) condensation reaction in the pressence of a sodium carbonate catalyst (Figure 1.2). By varying the amount of water added to this reaction it is possible to

control the eventual pore size distribution from about 4 nm up to 40 nm. Also, once the pyrolized gel is obtained, it is possible to control the surface chemistry of carbon xerogels. By treating it under oxidizing or reducing conditions the amount of surface oxygen can be varied, making it a versatile support in terms of binding sites for a catalytic phase. [29]

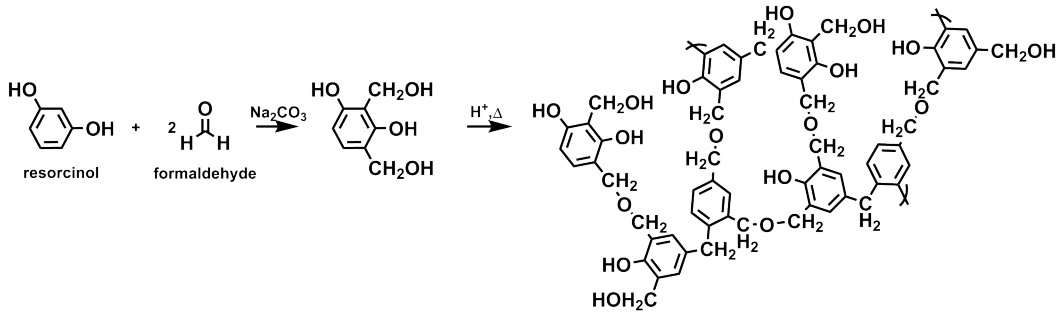

Figure 1.3 – *Schematic representation of the resorcinol formaldehyde condensation process. Sodium carbonate is added in a catalytic amount to activate the RF mixture towards polymerizing. The reaction is performed in water and by varying the organics:water ratio the final pore size of the gel can be controlled.*

While the inert nature of carbon xerogels is essential for this research, there is one important drawback. The material is so non-reflective that any analysis method based on light (e.g. IR, UV-Vis, Raman, etc.) can not be used. [30] This means other methods will have to be used to characterize the prepared catalysts.

1.5.2 High surface area graphite

High surface area graphite, or HSAG, is a mesoporous crystalline graphitic material consisting of small graphite particles. [31] HSAG can be obtained by mechanical modification of natural graphite (e.g. ball-milling) increasing the surface area up to ~500 m^2 per gram. [32;33] The small graphite particles consist of graphitic planes, which are more or less randomly ordered. This could give rise to different pore systems due to the morphology of the material. Within the graphite particles, can be found with a narrow PSD, while coalescing particles could give rise to interparticle porosity, leading to larger pores (Figure 1.4).

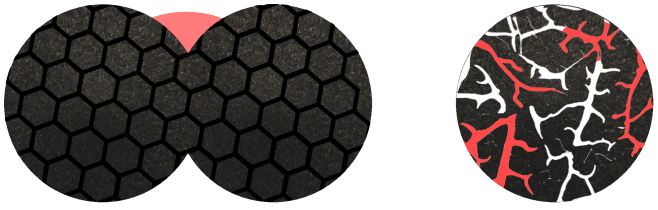

Figure 1.4 – *Depending on the morphology and orientation of the graphitic planes, different kinds of porosity could arise in HSAG.*

HSAG can accommodate heteroatoms on its surface and will readily undergo surface modifications by, for example, oxidative or reductive treatments.[34] The HSAG materials used in this project are commercially available and have well defined surface areas and pore size distributions.

1.5.3 Non-porous graphite

Since the project revolves around nanoconfined sodium alanate, it is desirable to synthesize a catalyst where nanoconfinement is physically impossible as to verify the (positive) effects nanoconfinement is supposed to have. For this purpose, non-porous graphite can be used. Like HSAG, it has a graphitic structure, but because it lacks porosity the sodium alanate will be deposited on the graphite surface. Because of this the sodium alanate crystallite size is expected to be larger and the catalyst will probably be more prone to sintering. Therefore, it is expected that the sodium alanate phase will show properties more comparable to bulk and the thermodynamics are expected to be less favourable for hydrogenation reactions.

Chapter 2

Experimental

2.1 Support preparation

2.1.1 Carbon xerogel

The carbon xerogels were prepared according to a procedure that has been used in the group before[35], based on research first published in 1989[36]. For each batch of xerogel, 8.65 g of resorcinol (78.5 mmol; ACS reagent, ≥99.0%; Sigma Aldrich), 12.89 g of formaldehyde (159 mmol; ACS reagent, 37 wt. % in H_2O, contains 10-15% methanol as stabilizer; Sigma-Aldrich) and 0.017 g of sodium carbonate (0.16 mmol) was dissolved in 12.00 g of distilled water while stirring. When weighing the exact amounts of reactants, it was made sure that the organic weight fraction of the solgel was always 40%, which should lead to xerogels with a 20 nm average pore size. The resulting solutions were transferred into teflon autoclaves and aged at room temperature for 24 hours. The autoclaves were then placed in an oven at 60 °C for 24 hours and subsequently 90 °C for 72 hours.

The resulting solid phase had a deep red/orange color. These organic gels were crushed in a mortar and soaked in acetone to exchange any residual water in the pores. The soaking step was repeated 3 times, with fresh acetone, for respective periods of 1 hour, 1 hour and 4 hours. After allowing the soaked gels to dry in air, they were pyrolized in a tubular oven at 800 °C under argon flow for a 10 hour period to remove any organic groups in addition to oxygen and water. The resulting black gel was transferred to an argon glovebox (≤0.1 ppm O_2 and H_2O) where it was crushed to a fine powder and stored for further use.

2.1.2 Graphitic supports

Commercially available HSAG (Timcal Ltd., Switzerland) with a surface area 100, 300 or 500 m^2/g was dried in a tubular oven under argon flow for 4 hours at 500 °C to remove any water and oxygen. The dried graphite was transferred to an argon glovebox (≤0.1ppm O_2 and H_2O) for storage until further use. Commercially available non-porous graphite (KS-6, Timrex) with a surface area of 20 m^2/g was treated in the same way.

2.1.3 Surface modifications

To investigate the influence of different surface groups on the carbon support, batches of CX-20 and HSAG-500 were treated under reducing or oxidizing conditions.

Reducing the supports was done by drying overnight at 200 °C under argon flow in a tubular oven. Then the temperature was raised to 600 °C for 2 hours, while flowing hydrogen. The samples were allowed to cool and were transferred to an argon glovebox for storage. The reduced supports will be referred to as CX-H(CX-20) and HSAG-H(HSAG-500).

The oxidative treatment was performed by heating under reflux a mixture of carbon support and 65% nitric acid (50 mL/ g Carbon) to 80 °C for 110 minutes under constant stirring. After cooling down the mixture was filtered and the carbon washed with distilled water until the filtrate had a neutral pH (pH 6-7). The carbon was then dried overnight at 200 °C under argon flow in a tubular oven and transferred to an argon glovebox for storage. The oxidized supports will be referred to as CX-Ox(CX-20) and HSAG-Ox(HSAG-500).

2.2 Support characterization

2.2.1 Nitrogen physisorption

Nitrogen physisorption isotherms were obtained using a Micromeritics ASAP 2020. Measurements were done at 77 K by cooling with liquid nitrogen. Approximately 50 mg of carbon support was used per measurement. The BET surface areas and BJH pore size distributions were calculated from the adsorption branch of the isotherm. The samples did not need any pre-treatment since storage and preparation in an argon glovebox ensured they would be already dried.

The prepared catalysts were characterized with nitrogen physisorption as well, in order to be able to calculate the decrease in pore size and surface area compared to the pristine support materials.

2.2.2 Acid/base titration

The supports that were surface treated under either reductive or oxidative conditions were characterized by acid- and base titration and compared to the pristine support material in terms of pH, acid sites per nm^2 and basic sites per nm^2. The titrations were performed on an automated titration setup, where approximately 25 mg of support material was suspended in a 0.1 M KCl solution and titrated with 0.0100 M NaOH solution

for acidic and 0.0100 M HCl solution for basic site determination. For the surface area of every support the nitrogen physisorption data was used to be able to determine the amount of acidic and basic sites relative to the surface area.

2.3 Catalyst preparation

In the remainder of this thesis multiple catalysts will be discussed. They will be referred to as: 'Preparation method'-'support'-'$NaAlH_4$ loading' e.g.: MI-CX20-20 is a melt infiltrated catalyst consisting of 20 wt% $NaAlH_4$ on carbon xerogel with a 20 nm average pore diameter.

2.3.1 Melt infiltration

All melt infiltrations were performed under inert conditions in stainless steel autoclaves. In an argon glovebox ($\leq$0.1ppm O_2 and H_2O)typically, 1 g of carbon support and 0.25 g $NaAlH_4$ (Hydrogen-storage grade, 93%; Sigma Aldrich) were mixed by grinding them together in a mortar for approximately 2 minutes. The catalyst mixture was then transferred into a graphite crucible which was put in an autoclave and sealed. The autoclave was pressurized to 80-100 bar with hydrogen and heated to 150 °C (5 °C/min, 10 minute dwell time), then to 180 °C (1 °C/min, 15 minute dwell time). Above this temperature the sodium alanate melts and is forced into the pores of the support by a combination of capillary force and external pressure. After 15 minutes the autoclave was allowed to cool down and placed back into the argon glovebox, where the prepared catalysts were stored for further use.

Some catalysts were made in batches of 0.5 g or 2 g or with a different support/$NaAlH_4$ ratio (prepared loadings: 5, 10, 20 and 40 wt.%) using the same procedure. Also, deuterated catalysts were prepared by pressurizing with deuterium instead of hydrogen.

2.3.2 Incipient wetness impregnation

For catalyst impregnation the carbon support and sodium alanate were transferred to a nitrogen glovebox ($\leq$1ppm O_2 and H_2O). Sodium alanate was dissolved in dry THF to serve as impregnation solution, however, this yielded a turbid, grey mixture indicating impurities. Therefore, a batch of sodium alanate was purified by adding a large excess of THF after which the grey solid was filtered off and the THF was allowed to fully evaporate under vacuum.

A precise amount of purified sodium alanate was dissolved in THF, taking into account the pore volume of the support, to obtain a weight loading of 5% $NaAlH_4$/C per impregnation cycle. For example: the catalyst IWI-CX20-5% was prepared with 1.00 g of CX-20 (pore volume 0.84 mL/g) using 0.84 mL of a solution of 1 mL THF containing 0.060 g $NaAlH_4$. After impregnation the catalysts were dried under vacuum at -40°C

by using a dry-ice/acetonitrile bath. The low drying temperature was used to ensure evaporation of THF without the chance of the sodium alanate already releasing hydrogen prematurely. For higher catalyst loadings the process was repeated 2-4 times, to produce the catalysts IWI-CX-5%, IWI-CX-10% and IWI-CX-20%, which were stored at -20°C under nitrogen atmosphere.

2.4 Catalyst characterization

2.4.1 X-ray diffraction

X-ray diffractograms were obtained using a Bruker AXS D8 Advance 120 (Co-K_α radiation source), using an airtight sample holder that was prepared in the glovebox. All measurements were performed with a 2θ increment of 0.1 °, measuring 1 second per point. The range of the measurements was from 20-100 °2θ while rotating the sample at 15 rpm. The resulting diffractograms were compared to that of bulk sodium alanate. Since nanoconfinement prevents long range crystallinity, a successful melt-infiltration can be recognized by the disappearing of the $NaAlH_4$ peaks. Additionally, aluminium peaks appeared for all prepared catalysts. Crystallite sizes were not determined, since only the aluminium peaks recurred in every sample and the difference in crystallite sizes were all within the margin of error when compared across different loadings, supports and preparation methods. By normalizing diffractograms to the carbon signal however, it was, in some cases, possible to estimate the amount of crystalline sodium alanate left in the catalyst and thus the amount of sodium alanate that really entered the pore system of the support by comparing to a 20 wt% physical mixture of $NaAlH_4$/CX-20 (or HSAG-500).

2.4.2 Temperature programmed hydrogen desorption

Temperature programmed desorption was performed using a Micromeritics Autochem II equipped with a TCD detector. The temperature program used was heating from room temperature to 400-500 °C with an increase of 5°C/min using argon as a carrier gas, unless stated otherwise. For some measurements a mass spectrometer was connected to the TPD for analysing the desorption products. The sample for MS was automatically taken before the gas-flow reaches the TCD, but control experiments pointed out that this does not influence the TPD results. Different TPD profiles can be compared by looking at the onset and peak temperatures for hydrogen desorption. Bulk sodium alanate for example has a desorption onset of $\sim$ 170 °C and a maximum desorption rate at $\sim$ 260 °C. Also, by integrating the hydrogen release over time, it is possible to calculate the total amount of hydrogen released in cm^3 per gram $NaALH_4$ (Figure 2.1). By dividing by the temperature ramp speed the integration can be performed without having to convert the horizontal axis to time units and by assuming the gas has cooled to 25 °C by the time it reaches the detector the hydrogen volume can be converted to an estimated weight

percentage of hydrogen released relative to the sodium alanate using the ideal gas law. In further figures only the volume of hydrogen released and the weight percentage this accounts for will be indicated.

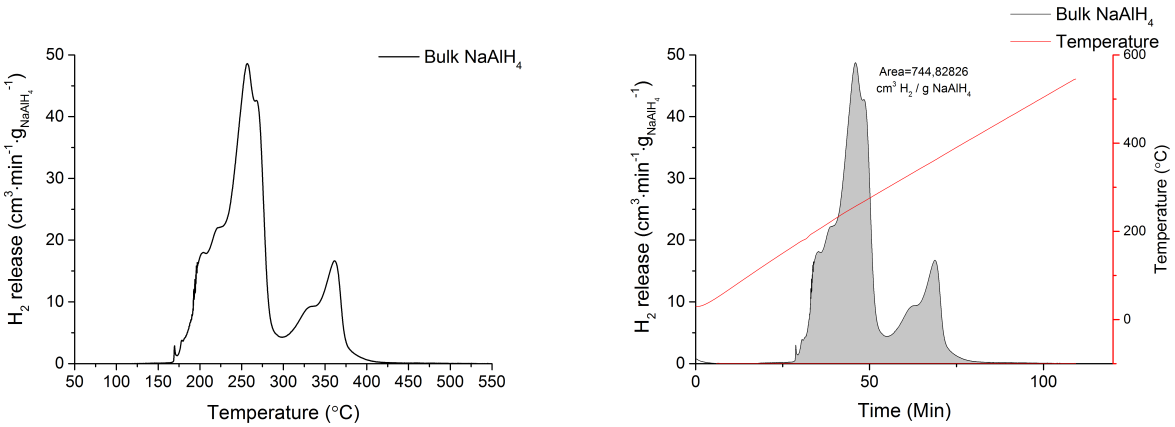

Figure 2.1 – Left: *TPD profile of bulk sodium alante, showing a desorption onset at /sim 170 ˚C and a maximum desorption rate at ∼ 260 ˚C.* Right: *Integrating the desorption over time yields the volume of desorbed hydrogen per gram of sodium alanate. Using the ideal gas law, assuming the temperature at the detector is 298 K this amounts to 6.14 wt% of hydrogen released: 90% of the theoretical maximum.*

2.5 Catalytic testing

2.5.1 Hydrogenation of diphenylacetylene

The standard reaction to test the activity of the differently prepared catalysts was the hydrogenation of diphenylacetylene (DPA, Figure 2.2). This is a 2-step reaction that can go through either the cis-stilbene or trans-stilbene intermediate to reach bibenzyl (BB). Previous research has shown that isomerization from cis- to trans-stilbene is a catalysed reaction as well, while the reverse reaction does not take place. Also, the benzene rings remain intact as sodium alanate is not strong enough of a reducing agent to break the aromaticity. The DPA used for these reactions (Sigma Aldrich, 98%) was dried under vacuum for at least 4 hours before being stored in a nitrogen glovebox and only left the glovebox in the sealed reaction vessels.

2.5.2 Reaction conditions

Reactions were performed in a 300 mL stainless steel autoclave (OA), for later reactions the autoclave was cleaned in a sonic bath after every reaction (CA) and reactions were performed using a new autoclave(NA) and a smaller 50 mL autoclave(SA). All reactions were performed using ∼5 mmol of substrate, ∼0.27 g of catalyst (1 mmol $NaAlH_4$) and a

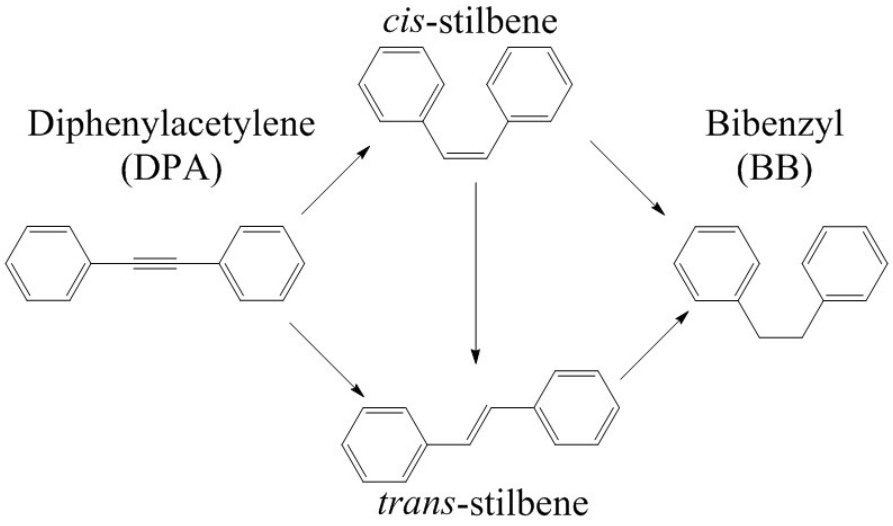

Figure 2.2 – *Standard reaction for catalyst optimization. Diphenylacetylene is hydrogenated via one or both of its intermediates to Bibenzyl. Note that the reaction from cis-stilbene to trans stilbene is also catlyzed by sodium alanate, but not the other way aroud.*

known amount of dodecane as internal standard, all dissolved in 180 mL of cyclohexane. For reactions in the small autoclave these amounts were 6 times smaller.

All reactions were prepared in a nitrogen glovebox to prevent air or water contamination. The sealed autoclaves were pressurized with 80-100 bar of hydrogen and heated to 100-250 °C for 4-48 hours. The exact pressures, temperatures and durations will be given per reaction in the results chapter if necessary. Sampling was only done for the large autoclaves. Two sampling methods were used: 0.6 mL samples by a time programmed autosampler and manual sampling using a double valve construction to retain the reaction pressure. In both cases the sampling line was flushed before the taking of each sample.

2.5.3 Substrate screening

Multiple organic substrates containing C=C bonds were used to learn more about the capabilities of sodium alanate as a hydrogenation catalyst. These reactions were performed with HSAG-500 supported sodium alanate (unless stated otherwise), since these catalysts are easier to synthesize and more reproducible since they can all be made from the same batch of HSAG.

To find out whether the nature of the C=C bond influences reaction speed and/or catalyst activity, 4 different C_8H_{16} molecules were tested with a different degree of substitution on the double bond (Figure 2.3). By using a mono-(1-octene, Sigma Aldrich,

98%), di-(trans-4-octene, Sigma Aldrich, 98%), tri-(2,4,4-trimethyl-2-pentene, Sigma Aldrich 99%) and tetra-substituted (2,3,4-trimethyl-2-pentene, Sigma Aldrich, 96%) double bonds without varying the molecular formula it might be possible to learn something about the catalyst activity towards different systems. The same reaction conditions were used as for tests with DPA using 5 mmol of substrate and 1 mmol $NaAlH_4$ at 80-100 bar hydrogen pressure and 190 °C for 4 hours.

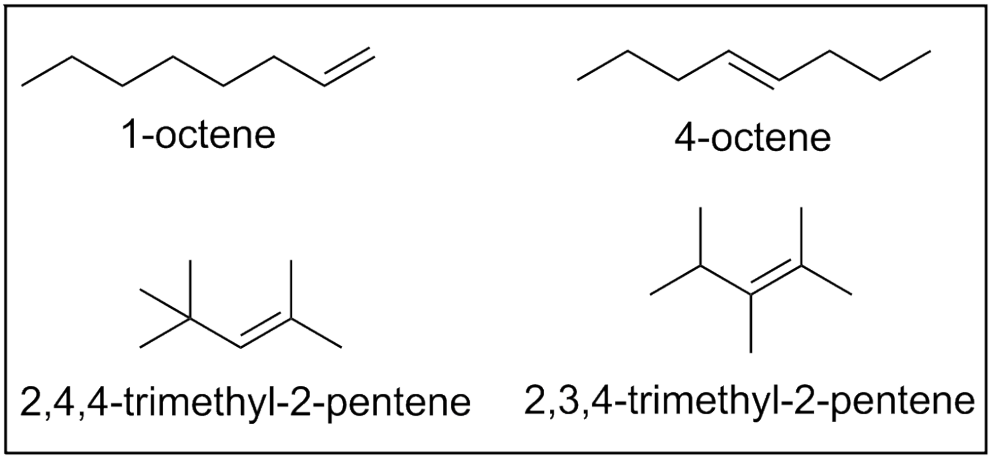

Figure 2.3 – *C_8H_{16}substrates*

Two oxygen containing substrates (trans-chalcone, Sigma Aldrich, 97% and allyl methyl ether, Sigma Aldrich, 97%) were tested to find out whether these could be hydrogenated or if they deactivate the catalyst (Figure 2.4).

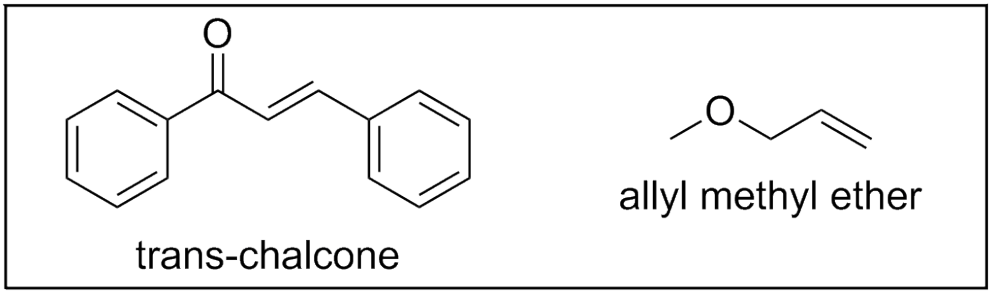

Figure 2.4 – *Oxygen containing substrates*

2.5.4 GC analysis

Analysis of the DPA to BB reaction was done on a Shimadzu GC-2010 gas chromatograph equipped with an Agilent J&W CP-Wax 57 CB column (Length: 25 m, ID: 0.25 mm, Film: 0.20 μm) and an FID detector. The program used had a starting temperature of 60 °C, which was held for 5 minutes. Then the temperature was raised with 10 °C/min to 210 °C, which was held for 15 minutes.

Analysis of norbornylene was performed using a Varian 430-GC gas chromatograph equipped with an Agilent J&W VF-5ms column (Length: 30 m, ID: 0.25 mm, Film: 0.25 μm), Agilent medium polar retention gap and an FID detector. The program used had a starting temperature of 40 °C, which was held for 5 minutes. Then the temperature was raised with 20 °C/min to 240 °C, which was held for 10 minutes.

For the substrate screening, GC-MS was used to verify the reaction products. This was done on a Shimadzu GC-2010 gas chromatograph equipped with an Agilent J&W CP-Wax 57 CB column (Length: 25 m, ID: 0.25 mm, Film: 0.20 μm) coupled to a Shimadzu GCMS-QP2010 quadrupole MS. The GC program used had a starting temperature of 40 °C, which was held for 5 minutes. Then the temperature was raised with 40 °C/min to 290 °C, which was held for 10 minutes.

2.5.5 Norbornylene & isotope labelling

To learn more about the reaction mechanism, three mechanistic experiments were run with 5 mmol norbornylene as substrate. The first reaction to test catalytic activity for norbornylene hydrogenation. The second experiment was run with a deuterated catalyst in deuterium atmosphere and was characterized using a 400 MHz Oxford Instruments NMR to see how the deuterium is added to the double bond. A last experiment was run with norbornylene in deuterium atmosphere. This experiment was designed to keep track of the time it takes to incorporate deuterium in the product. If deuterium incorporation is instant, the hydrogenation reaction likely takes place in the atmosphere, whereas an induction period would mean reaction takes place on the catalytic surface.

The deuterated catalyst was characterized by TPD-MS, to see whether the preparation was successful. Also, a thermogravimetric analysis (TGA) measurement was done under 50 bar of H_2, increasing the temperature from 40 to 190 °C with 10 °C per minute, which was held for 25 minutes. The weight loss was calculated and compared to that of the standard sodium alanate catalyst, to have a better look at the minimal hydrogen desorption conditions under circumstance better resembling those during reaction.

2.5.6 Table of catalysts

All the catalysts that will be discused in the upcomming chapters have been summarized in Table 2.1. For every catalyst the preparation method, support and sodium alanate weight loading are given. H and Ox behind support names mean they have been surface treated under reductive or oxidative conditions respectively. D_2 behind the preparation method means it was carried out in deuterium atmosphere instead of hydrogen.

Catalyst	**Preparation method**	**Support**	**Weight loading (%)**
IWI-CX20-5	Incipient wetness impregnation	CX-20	5
IWI-CX20-20	Incipient wetness impregnation	CX-20	20
MI-CX20-5	Melt infiltration	CX-20	5
MI-CX20-10	Melt infiltration	CX-20	10
MI-CX20-20	Melt infiltration	CX-20	20
MI-CX20-40	Melt infiltration	CX-20	40
MI-CX20H-20	Melt infiltration	CX-20-H	20
MI-CX20Ox-20	Melt infiltration	CX-20-Ox	20
MI-HSAG-20	Melt infiltration	HSAG-500	20
MI-HSAGH-20	Melt infiltration	HSAG-H	20
MI-HSAGOx-20	Melt infiltration	HSAG-Ox	20
MI-NPG-20	Melt infiltration	NPG(KS6)	20
MI-HSAG-20D	Melt infiltration (D_2)	HSAG-500	20

Table 2.1 – *Summary of the most important variables between the catalysts that will be discussed in the upcomming chapters.*

Chapter 3

Results & Discussion

In this chapter the results of the conducted research will be shown and discussed. Because the mechanism and kinetics of hydrogenation over sodium alanate are still largely unclear, the reactions mentioned in this chapter will be compared on the time needed to reach 50% conversion of DPA. This is done, because up to 50% of conversion the reaction speed is close to constant and the DPA depletion almost linear against time. After 50% conversion, the isomerization and reaction of the cis and trans intermediates start playing an important role and the reaction speed of DPA no longer accounts for the major part of catalytic activity. When the comparison involves reactions that do not reach 50% conversion (e.g. for control experiments) they will be compared by the amount of conversion at the end of the reaction, unless mentioned otherwise.

3.1 Proof of catalytic activity

To be able to quantify any improvements made to the catalyst a baseline had to be set. To do this, first the supposed catalyst had to be proven active. Sodium alanate was confirmed to be the active component by running two blank experiments, first without any catalyst at all (Figure 3.1, left) and second with only the support material to exclude the support from having catalytic activity (Figure 3.1, right). Both converting only minimal amounts of DPA under the standard reaction conditions. For the blank reaction containing support material, 0.27g of HSAG was used rather than CX-20, because of the easy availability of HSAG compared to the limited amount of CX-20 that was prepared. Both reactions converted only about 15% of DPA, most likely driven by the high hydrogen pressure in combination with high temperatures. The total conversion of DPA was less than 15% in both cases and yielded no significant amount of BB. (Table 3.1)

Next, a reaction was prepared containing 0.27 g of MI-CX20-20 catalyst. The total amount of sodium alanate added to the reaction comes down to 1 mmol, while 5 mmol of DPA was added. Since DPA has a triple bond this comes down to 10 mmol of bonds that can be hydrogenated: a $10:1$ ratio should the reaction run to completion. Figure 3.2 and Table 3.1 show the improvement in DPA conversion compared to the blank experiments: nanoconfined sodium alanate clearly has a positive effect on the reaction.

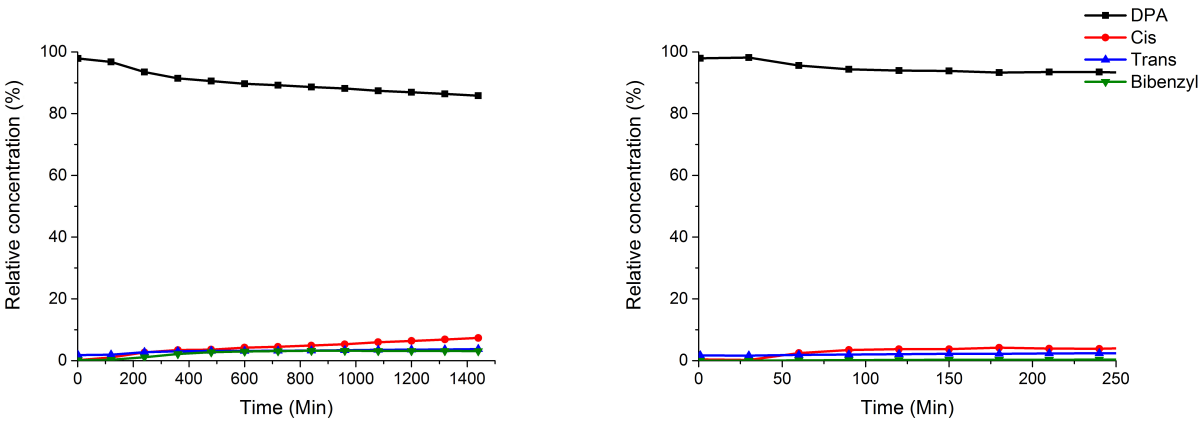

Figure 3.1 – Left: *A blank experiment without any catalyst.* Right: *A blank experiment with 0.27g of HSAG added to the reaction mixture.* Conditions: *5 mmol DPA, 180 mL cyclohexane, 150 ˚C, 100 bar H_2.*

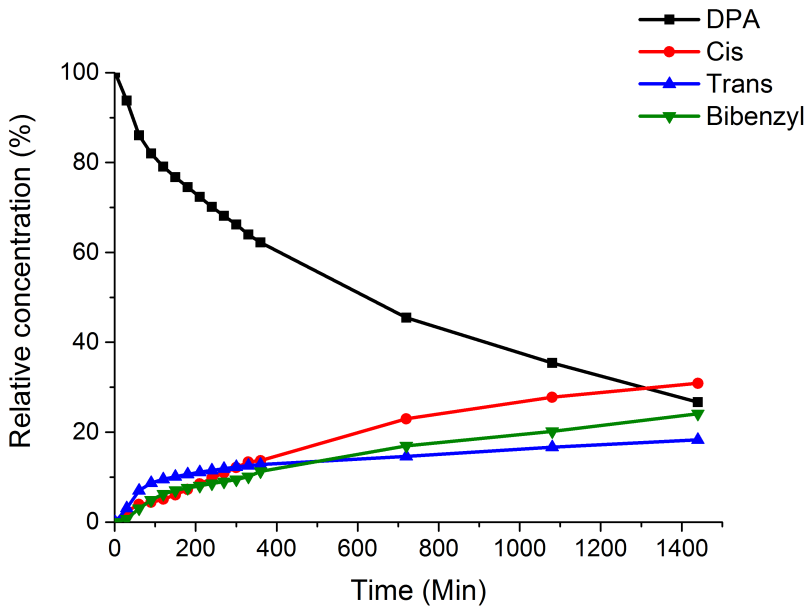

Figure 3.2 – *A reaction with 0.27g of a MI-CX20-20 catalyst , shows that nanoconfined sodium alanate is indeed catalytically active in the hydrogenation of DPA.* Conditions: *1 mmol $NaAlH_4$, 5 mmol DPA, 180 mL cyclohexane, 150 ˚C, 100 bar H_2.*

		Yield (%)		
Reaction	**DPA Conversion (%)**	**Cis**	**Trans**	**BB**
Blank	14.15	7.35	3.72	3.09
Blank + HSAG	11.97	6.02	4.39	1.56
MI-CX20-20	73.30	30.88	18.32	24.10

Table 3.1 – *Results of blank experiments after 24 hours of reaction compared to a reaction with catalyst. This shows the support alone has no catalytic activity, but nanoconfined sodium alanate is catalytically active in DPA hydrogenation.*

Almost 75% of the DPA is hydrogenated and almost a quarter of the starting material is converted to BB. This means roughly 5 mmol of double bonds have been hydrogenated, 5 times the stoichiometric equivalent of the sodium alanate added, proving the catalytic activity of nanoconfined sodium alanate in hydrogenation of DPA.

The first results were promising, but reactions took 24 hours to complete and while catalytic, the turnover number of only 4.9 seems to indicate either rapid catalyst deactivation or an inefficient reaction. By experimenting with several variables in catalyst preparation, support properties and reaction conditions it was attempted to gain a better understanding of the system whilst simultaneously improving turnover and yields.

3.2 Catalyst optimization

To optimize the catalytic performance, a closer look was taken at different variables in the catalyst preparation process. To start with, two different methods of catalyst preparation were tested to explore different ways of contacting the sodium alanate phase with the carbon support. The best method was then used to test different carbon supports, both with and without surface modifications. Finally, the amount of sodium alanate was varied to find an ideal sodium alanate/performance ratio. The results of these experiments will be discussed in the sections below. Unfortunately, there was not enough time to explore every possible path for optimization, more on this can be found in the *Outlook & Reccomendations* chapter.

3.2.1 Method of sodium alanate loading

To determine the most efficient method of catalyst preparation, four catalysts were tested. Melt infiltration was compared to incipient wetness impregnation for $NaAlH_4$ loadings of 5 wt.% and 20 wt.% on CX-20. When characterized with XRD and normalized to the carbon signal, the sodium alanate peaks strongly decrease in intensity, or disappear altogether (Figure 3.3). Only for the MI-CX20-20 catalyst a significant

amount of crystalline sodium alanate can still be seen, which might mean that the pores can only be filled to a certain degree, after which the rest of the sodium alanate remains on the outside of the support. Furthermore, in the melt infiltrated catalysts, a set of new peaks appears at 45, 52, 77 and 94 °2θ. These peaks are caused by a crystalline aluminium phase that is apparently produced during melt infiltration. The formation of this phase can have several causes, e.g. evaporation of sodium during the heating process or an excess of aluminium in the sodium alanate stock, but the exact cause is beyond the scope of this project and will be shortly discussed in the *Outlook & Reccomendations* chapter. From these results, the IWI catalysts would be expected to have a higher activity, since the sodium alanate dispersion is likely better as no crystalline material can be seen with XRD.

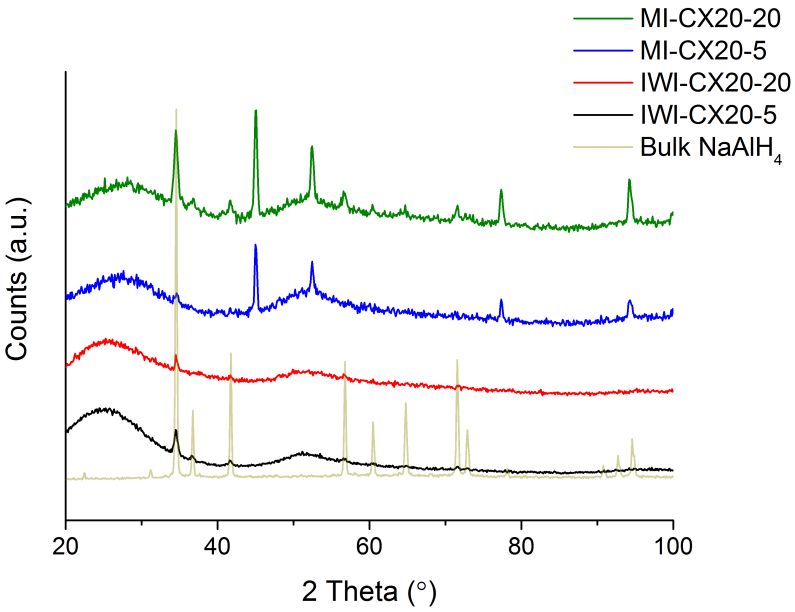

Figure 3.3 – *The XRD diffractograms of the MI and IWI catalysts compared to that of bulk sodium alanate. The sodium alanate peaks show a large decrease in intensity. For the melt infiltrated catalysts a crustalline aluminium phase can be seen, the exact cause of which is unclear.*

The TPD results of the 4 catalysts contradict the expectations from XRD (Figure 3.4). Even though the IWI-CX20-20 catalyst does not show any significant amount of crystalline material, the hydrogen release is only 3-10% of the amount released by the other catalysts and at a higher temperature than any of the other catalysts. Also, a broad peak can be seen from 25 to 170 °C, which could be caused by THF that was still complexed to the sodium alanate. When comparing to the TPD of bulk sodium alanate, (Figure 2.1) the remaining three catalysts show a significant improvement in onset and peak temperatures of hydrogen release of approximately 60 °C. Also, the multi-step hy-

drogen release in bulk sodium alanate, which can be explained by looking at Figure 1.1, is largely absent for nanoconfined sodium alanate. Either the peaks have merged into one, or only the first hydrogen desorption step takes place. Looking at the total amount of hydrogen released, the second explanation seems the more likely one as this was also suggested in literature. [14;23]

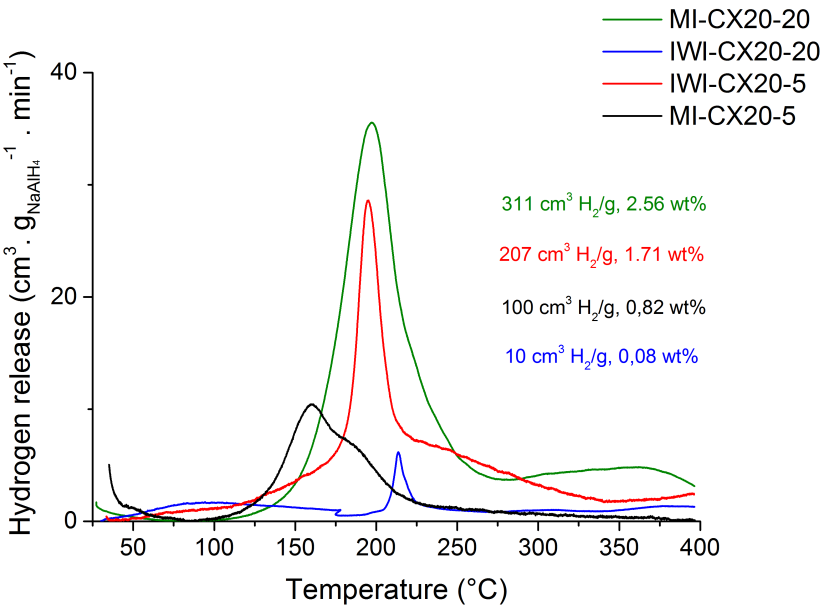

Figure 3.4 – *The TPD profiles of the MI and IWI prepared catalysts show high hydrogen desorption and lower desorption temperatures for the melt infiltrated catalysts. The 5 wt% IWI catalyst is somwhere in the middle, but the 20 wt% IWI catalyst hardly releases any hydrogen at all. The indicated hydrogen release is relative to 1 g of sodium alanate.*

From TPD the melt infiltrated catalysts would be expected to perform better, as they release more hydrogen despite the XRD results showing they contain more crystalline sodium alanate. The MI-CX20-20 catalyst releases 2.56 wt% of hydrogen, as much as the other three combined and the MI-CX20-5 catalyst shows a desorption peak at a lower temperature of $\sim$ 150 °C. The explanation for this might partially be found in the nitrogen physisorption data for these catalysts (Figure 3.5). Weight loadings of 5 and 20 wt% of sodium alanate amount to 0.04 and 0.16 cm^3/g respectively. When looking at the remaining pore volume after impregnation, one can see that the melt infiltrated catalysts only have minimal pore blocking, while the incipient wetness impregnated catalysts show a drastic decrease in total pore volume. Once more, this might be accounted for by THF complexing to the sodium alanate and blocking the pores. When combining the physisorption and TPD results, it seems that the pores are being blocked so effectively that hydrogen can no longer desorb from sites deeper inside the pores. Alternatively, the THF-sodium alanate complex could cause a reduction in hydrogen desorption altogether.

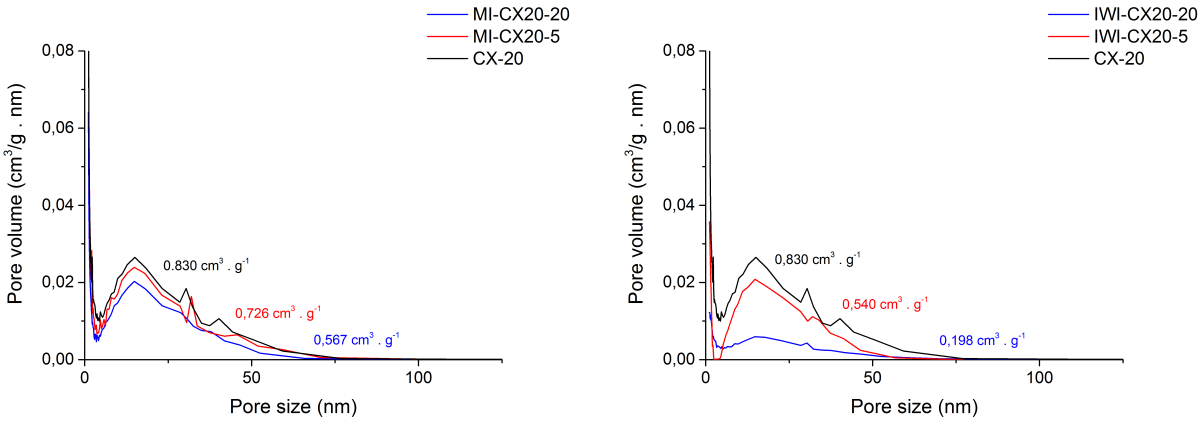

Figure 3.5 – *The nitrogen physisorption results of the MI and IWI catalyst show that the IWI catalyst suffer greatly from pore blocking, while the MI catalysts largely retain their open structure.*

The reaction profiles of the catalysts show that preparation by melt infiltration produces catalysts that are a lot more active than those prepared by incipient wetness impregnation, regardless of catalyst loading (Figure 3.6 and Table 3.2). There might be several reasons leading to this result, but the most likely problem with incipient wetness impregnation is the formation of a THF/$NaAlH_4$ complex. This complex supposedly does not decompose under the drying conditions (-40 °C under vacuum) causing the resulting catalyst to be largely inactive. This would also explain why the 20 wt.% IWI catalyst is in turn a lot less active than the 5 wt.% catalyst: because of multiple impregnation cycles, more THF could be retained in the carbon pore system, deactivating the sodium alanate phase completely.

		Yield (%)		
Reaction	**DPA Conversion (%)**	**Cis**	**Trans**	**BB**
IWI-CX20-5	35.15	21.59	4.16	9.40
IWI-CX20-20	4.61	2.15	1.83	0.63
MI-CX20-5	82.39	37.94	9.91	34.54
MI-CX20-20	73.30	30.88	18.32	24.10

Table 3.2 – *Results of the different preparation methods after 24 hours of reaction. (note that for IWI-CX20-20 the reaction took 30 hours, but no further reaction was observed.) The melt infiltrated catalysts clearly outperform those prepared by incepient wettnes impregnation.*

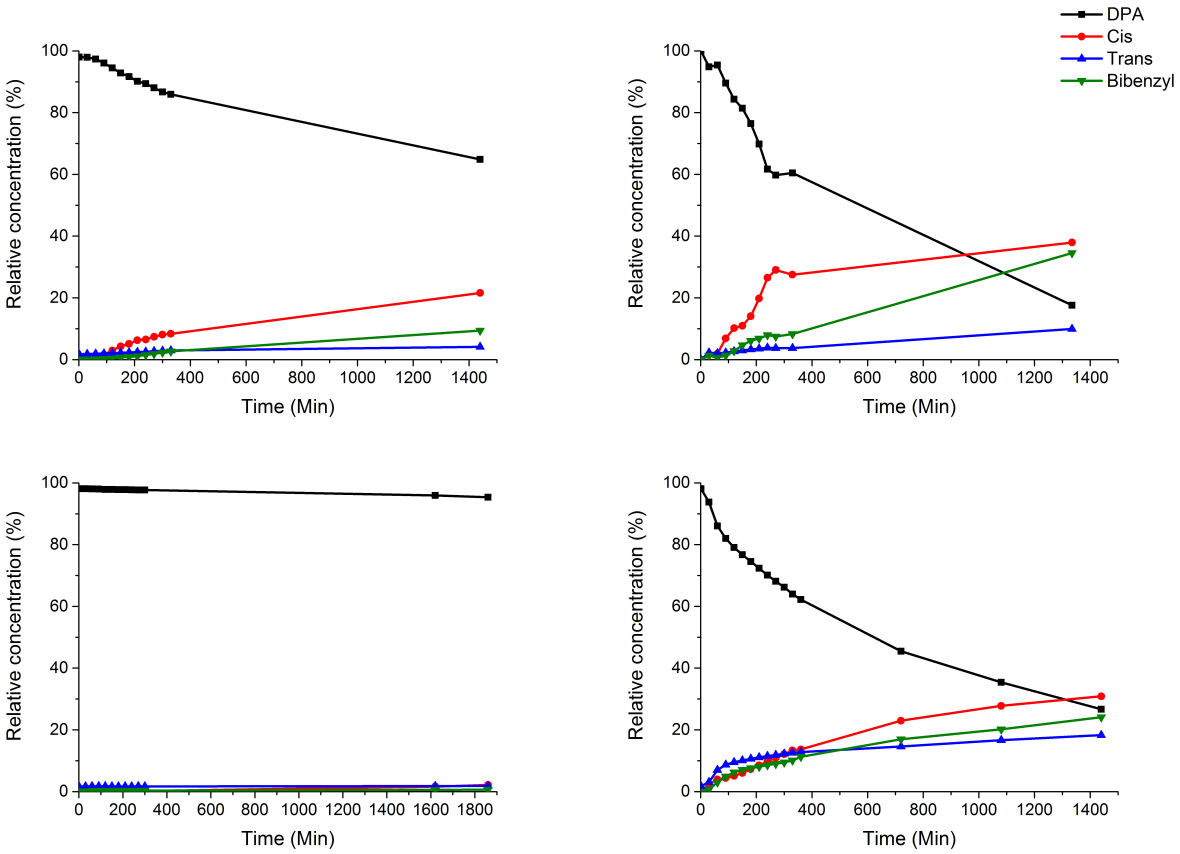

Figure 3.6 – Top left: *5 wt.% $NaALH_4$/CX-20 prepared by incipient wetness impregnation.* Top right: *5 wt.% $NaAlH_4$/CX-20 prepared by melt-infiltration.* Bottom left: *20 wt.% $NaALH_4$/CX-20 prepared by incipient wetness impregnation.* Bottom right: *20 wt.% $NaAlH_4$/CX-20 prepared by melt-infiltration.* Conditions: *1 mmol $NaAlH_4$, 5 mmol DPA, 180 mL cyclohexane, 150 ˚C, 100 bar H_2. The melt infiltration catalysts clearly outperform those prepred by incipient wetness impregnation.*

It was also attempted to do an incipient wetness impregnation using diethyl ether as solvent, but it was found that despite mention in literature sodium alanate does not sufficiently dissolve in diethyl ether. Preparation of HSAG or differently supported catalysts by incipient wetness impregnation was not attempted, since the catalytic test results showed the technique to be inferior or (for the 5 wt.% catalyst) comparable to melt infiltration while being a lot less reproducible and more laborious.

3.2.2 Different supports

Initially three different carbon supports were tested: CX-20, HSAG-500 and NPG. The NPG catalyst was a control experiment to prove that nano confinement is essential for this catalyst and was not expected to be very active, since it lacks any relevant porosity. The CX-20 and HSAG-500 catalysts both are porous, but differ significantly in their pore size distributions. While HSAG-500 mainly has well defined pores of $\sim$ 6 nm, with only few larger pores, CX-20 has a wider PSD between 5 and 50 nm (Figure 3.8). The fourth catalyst that was prepared was identical to the MI-CX-20 catalyst in everything, except that the support was ground up in a mortar for 5 minutes prior to melt infiltration, to get support particles as small as possible. The reason for this experiment was to see whether particle size effects might be playing a significant role in this reaction.

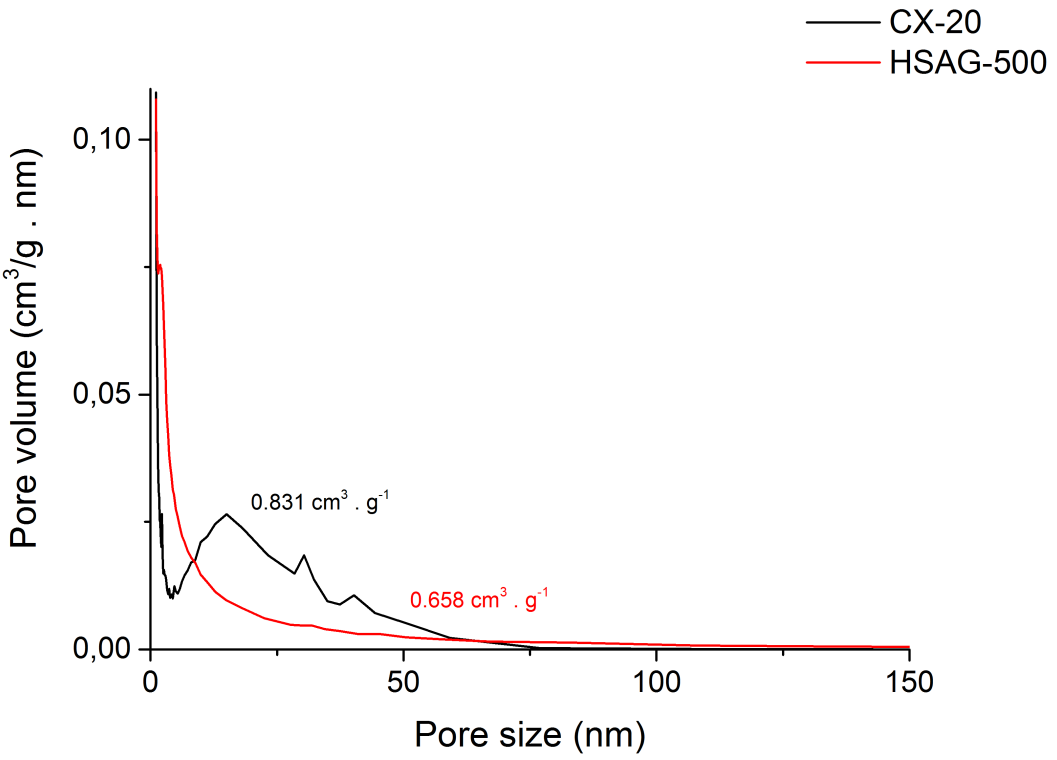

Figure 3.7 – *Nitrogen phyisorption shows that HSAG-500 has generally smaller pores and a narower pore size distribution compared to CX-20. The total pore volume of HSAG-500 is also slightly lower, but still sufficient to accomodate 20 wt% of sodium alanate.*

After melt infiltration nitrogen physisorption of the prepared catalysts was performed as well (except for the MI-NPG-20 catalyst, since the support had no porosity to start with, Figure 3.8) As with the previous MI catalysts, there seems to be some pore blocking, more for the HSAG catalyst than for the CX-20 catalysts, but the major part of the pore system is left intact. Pore filling is roughly equal for the ground up CX-20 compared to the original sample.

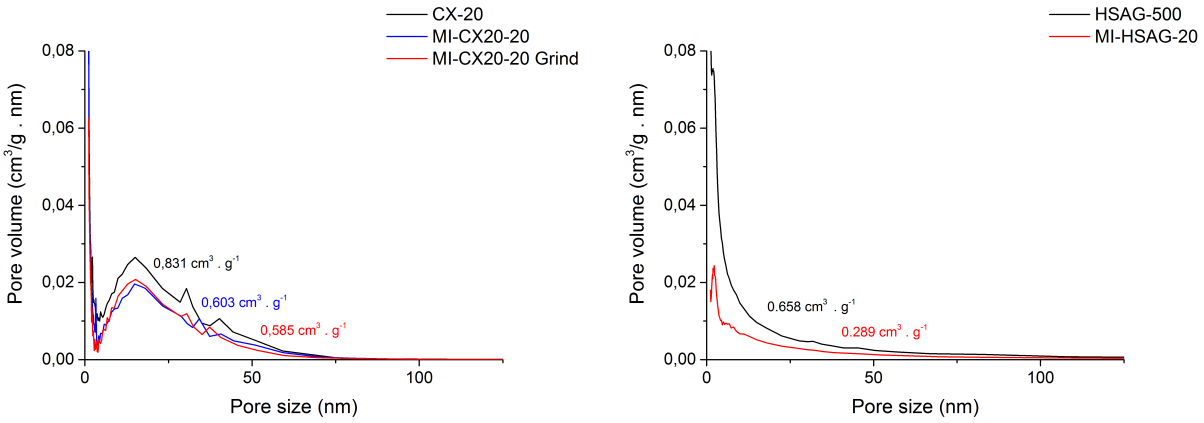

Figure 3.8 – *The nitrogen physisorption results of supports and catalysts show a decrease in pore volume upon melt infiltration. The decrease is larger than the 0.16 cm^3/g that is the volume of the added sodium alanate, indicating a small amount of pore blocking.*

When plotting the TPD profiles of these catalysts and integrating the hydrogen release over a temperature interval from 100-400 °C, a couple of interesting observations were made (Figure 3.9). As expected, the NPG supported catalyst shows the same behaviour as bulk sodium alanate. However, the total hydrogen release is 0.55 wt% higher than for bulk sodium alanate. This might either be caused by an unknown interaction with the NPG or by experimental error. When looking at the HSAG and CX-20 catalysts, the temperature of hydrogen desorption is significantly lowered by nanoconfining the sodium alanate. Compared to the HSAG, the CX-20 catalysts clearly show lower desorption onset and peak temperatures. Where we could not see significant difference between the ground up and original CX-20 in nitrogen physisorption, in TPD the catalyst on the ground up support clearly releases a lower amount of hydrogen.

The XRD diffractograms of the catalysts confirm these observations (Figure 3.10). The NPG supported catalyst shows a significant amount of sodium alanate being present in crystalline form. The HSAG en ground up CX-20 supported catalyst show a perfect impregnation: no crystalline sodium alanate is left and only the aluminium peaks can be observed. The peaks at 30 °2θ are caused by the crystalline graphitic carbon in the HSAG and NPG supports.

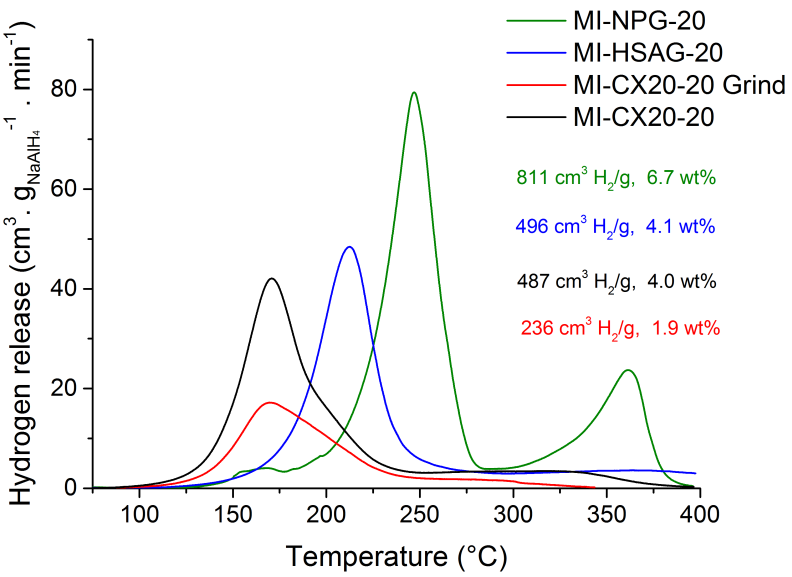

Figure 3.9 – *The TPD profiles of catalysts prepared with different supports show that onset andpeak temperatures of hydrogen release are significantly lowered by nanoconfing the sodium alanate, however, the amount of hydrogen released is also significantly lower.*

When comparing the TPD results with the results from catalytic testing on the time it takes to reach 50% DPA conversion, (Figure 3.11 and Table 3.3) multiple things can be concluded. First of all, the MI-NPG-20 catalyst never reaches 50% conversion, proving that, indeed, nanoconfinement of the sodium alanate is crucial to its catalytic activity. Secondly, while the original CX-20 catalyst does not perform very well compared to the HSAG, the ground up CX-20 surpasses it by a fair margin of ∼90 minutes. With the TPD results in mind, this is rather interesting. Both the CX-20 catalysts release their hydrogen at lower temperatures than the HSAG catalyst (∼ 170 °C versus ∼210 °C respectively) and the catalyst on ground up CX-20 releases significantly less hydrogen. Still, this seems to be the most active catalyst. This might mean that the interaction of sodium alanate with the carbon support causes it to release less hydrogen, but the hydrogen it does release is released in a reversible manner at lower temperatures. It is not clear whether the improved activity upon grinding the CX-20 is caused by a particle size effect or that the sodium alanate has better contact with the carbon phase due to the smaller particles, but catalyst activity clearly benefits when the catalyst particles are smaller. The XRD diffractograms show that impregnation is more complete on ground up CX-20 compared to the original CX-20, so enhanced sodium alanate/carbon contact is a likely explanation. Further research is needed to point to the exact cause of this effect.

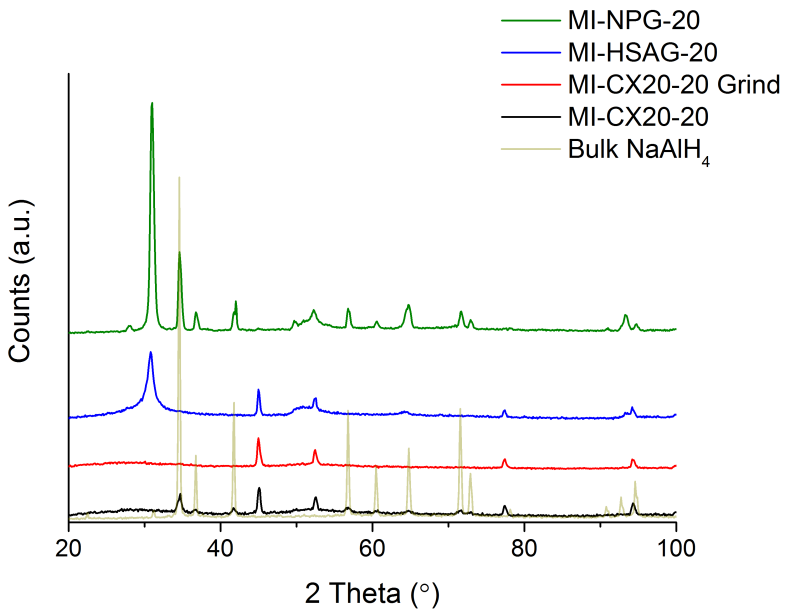

Figure 3.10 – *The XRD results of the differently supported catalyst show that there is indeed no nanoconfinement in the NPG catalyst. The original CX20 also shows some left-over crystalline sodium alanate. The ground up CX20 and the HSAG supports only show some crystalline aluminium, indicating near perfect infiltration of the sodium alanate into the pores. The peaks around 30 °2θ are caused by crystalline graphitic carbon phases.*

		Yield (%)		
Reaction	**Time to 50(%) conversion (min)**	**Cis**	**Trans**	**BB**
CX20	970	14	15	21
Ground CX20	253	13	24	12
HSAG-500	346	7	33	11
NPG	N.A. (35.6%)	14.49	4.41	16.69

Table 3.3 – *Catalytic testing results of catalysts on different supports under standard reaction conditions at 150 °C. The results are compared on the time it takes to reach 50% DPA conversion.*

When also looking at the final phase of the reactions, the HSAG seems to retain a higher activity compared to the CX-20 catalysts, converting nearly 100% of the DPA and yielding significantly more BB. This could mean that HSAG supported sodium alanate is more stable in the long run. Further research will be needed to confirm this, but in this project we will stick to the ground up CX-20 supported catalysts, as they show the best initial reaction rate. From this point on ground up CX-20 will be referred to simply as CX-20, as the original CX-20 will no longer be used.

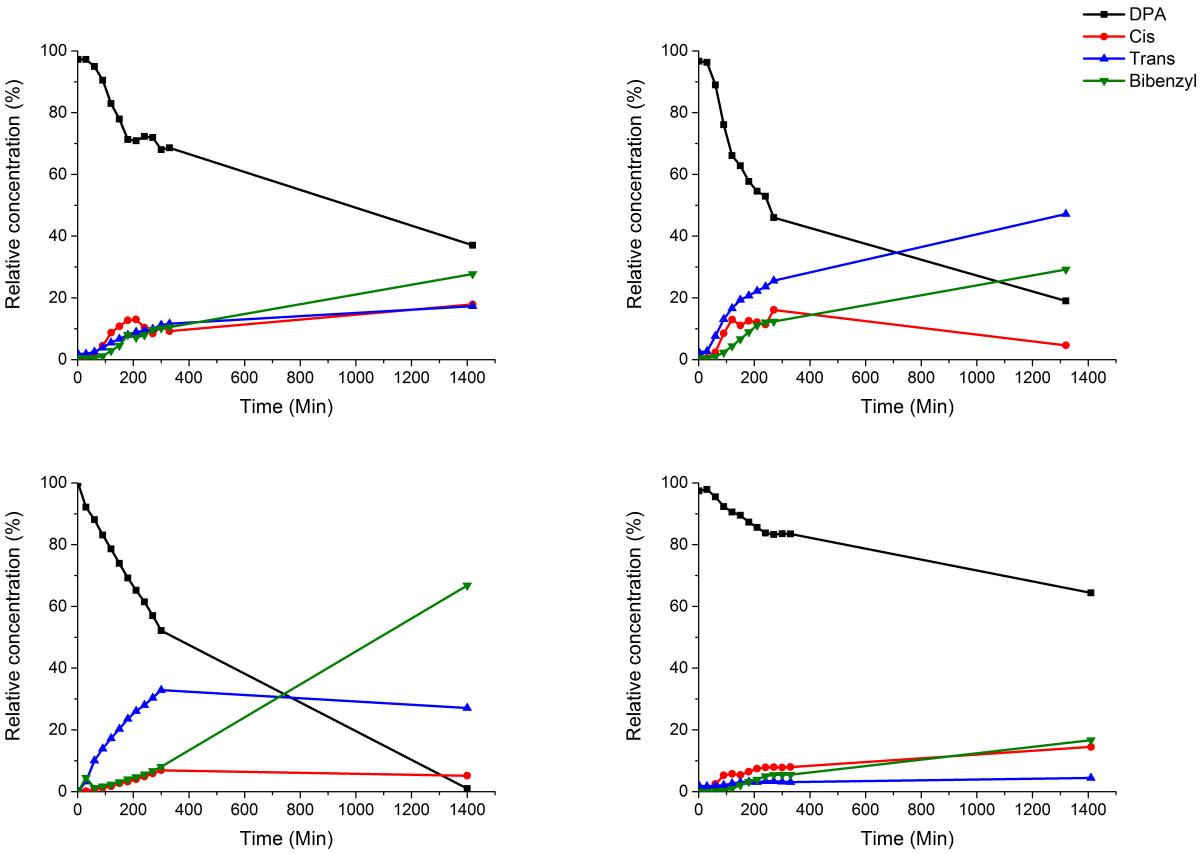

Figure 3.11 – *Catalytic testing results of catalysts on different supports.* Top left: *Original CX-20.* Top right: *Ground up CX-20.* Bottom left: *HSAG-500.* Bottom right: *NPG. The results are compared on the time it takes to reach 50% DPA conversion.* Conditions: *1 mmol $NaAlH_4$, 5 mmol DPA, 180 mL cyclohexane, 150 °C, 100 bar H_2.*

3.2.3 Surface modifications

To find out whether the support surface has any influence on the catalytic performance the oxidized and reduced CX-20 and HSAG-500 supports were melt infiltrated with 20 wt% of sodium alanate and put to the test. The treated supports were titrated with both, acid and base and compared to the pristine support materials. (Table 3.4) The CX-20 and HSAG-500 seem to follow the same trend: reductive treatment results in a slight increase in basic sites and a slight decrease in acidic sites, while oxidative treatment induces ten times more acid sites, destroying any basicity.

Nitrogen physisorption was performed to make sure the pore systems of the treated supports were not destroyed (Figure 3.12). Again, both support materials followed the same trend. Treating the supports under reductive conditions slightly decreased the total pore volume, while narrowing the PSD. This might be caused by the high temperature for a

Support	pH	Acid sites (/nm^2)	Basic sites (/nm^2)
CX20	8.2	0.013	0.140
CX20-H	8.4	0.010	0.148
CX20-Ox	4.5	0.145	N.A.
HSAG500	7.5	0.040	0.029
HSAG500-H	8.0	0.014	0.067
HSAG500-Ox	4.1	0.625	N.A.

Table 3.4 – *The amount of acid and basic sites per surface area was determined for the surface treated and pristine supports using titration. Oxidative treatment seems very effective, increasing the amount of acidic groups about 100 times, while reductive treatment does not seem to cause much change to the surface chemistry.*

prolonged amount of time during the treatment. Treating the supports under oxidative conditions had much the same effect, but to a larger extent. It makes sense that the total pore volume decreases in this case, since extra groups are added onto the surface of the supports.

After melt infiltration the prepared catalysts were measured with nitrogen physisorption again, but this time the result was unexpected. While the HSAG catalysts behaved according to expectations, showing a slightly lower total pore volume compared to the untreated support, the CX-20 catalysts showed an increase in total pore volume of 6% and 10% for the reductive and oxidative treatments respectively. These values are close to the edge of the error margin, but will be treated as experimental errors since the reason for this deviating behaviour could not be found and the nitrogen physisorption data shows that the pore structures are left almost completely intact when alternating the surface chemistry of the support materials.

With the pore systems of the catalysts intact the expectation was that the oxidized supports would make for better melt infiltrations. The reason for this is the ability of sodium alanate to anchor itself to oxygen containing sites on the support surface, meaning that more acidic sites provide more anchoring points and thus potentially more sodium alanate inside the pores as smaller particles. The reduced supports were not expected to be much different from the pristine materials, since the change in the amount of acidic and basic sites was orders of magnitude smaller than for the oxidated support materials. XRD diffractograms of the catalysts confirmed this expectation (Figure 3.13). Where the untreated and reduced supported catalyst show identical amounts of crystalline aluminium, the catalysts on oxidized supports show significantly less crystalline

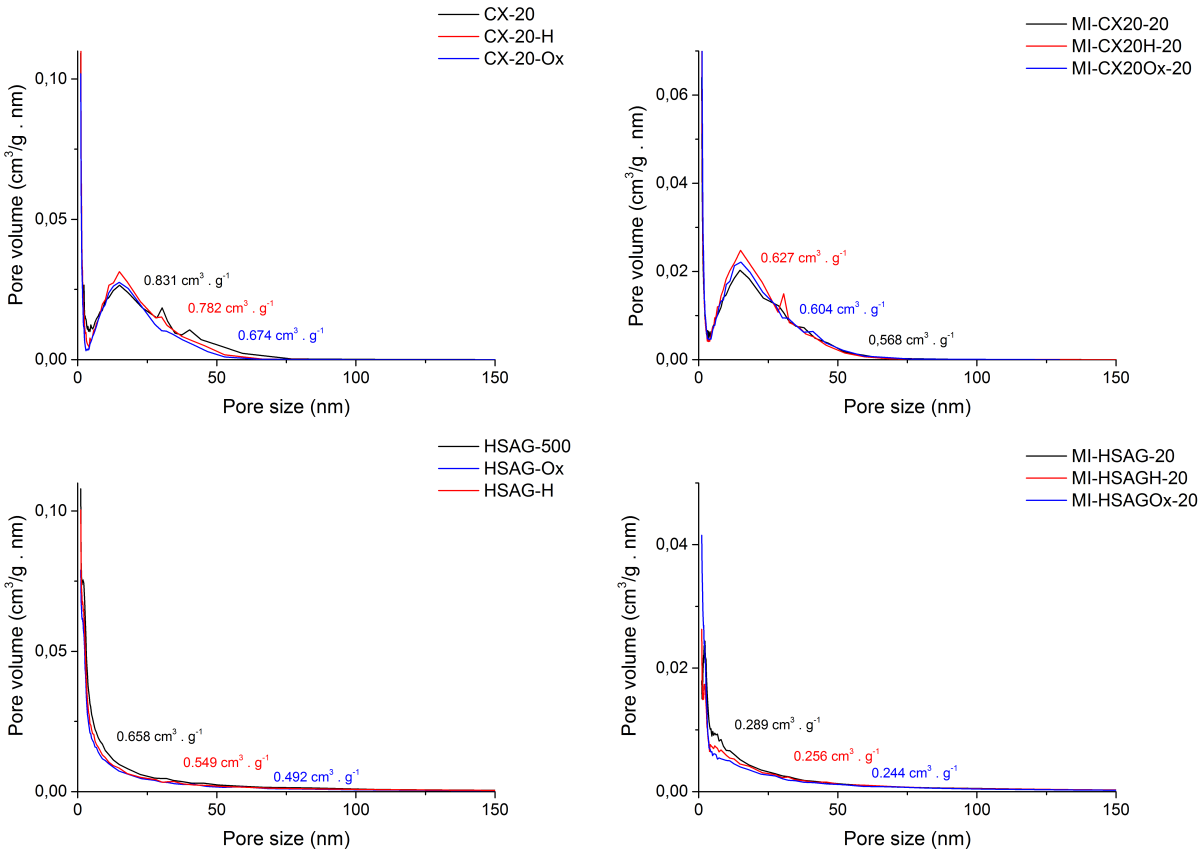

Figure 3.12 – *The nitrogen physisorption results of supports and catalysts after surface treatment show the pore structure is left intact during the surface treatment. The CX supported catalysts show slightly peculiar results in this experiment, the resaon of which could not be found.*

material. This does not mean they will automatically be better catalysts, since the oxygen containing sites could potentially oxidize part of the sodium alanate, rendering it inactive.

The TPD profiles of the catalysts on oxidized supports show a relatively low amount of hydrogen release, which could be caused by the suggested oxidation of sodium alanate. The amount of hydrogen released is significantly lower and the release temperature higher for the HSAG-Ox catalyst compared to the pristine HSAG catalyst. In the case of CX-20, the oxidized support even caused the catalyst to not release any hydrogen at all (Figure 3.14). It is not necessarily the case that only oxidation of the sodium alanate prevents these catalysts from releasing less hydrogen. The peak shift of the HSAG-Ox catalyst to higher values could indicate that the oxidic groups on the support surface bind the sodium alanate stronger, raising the energy required to make it release hydro-

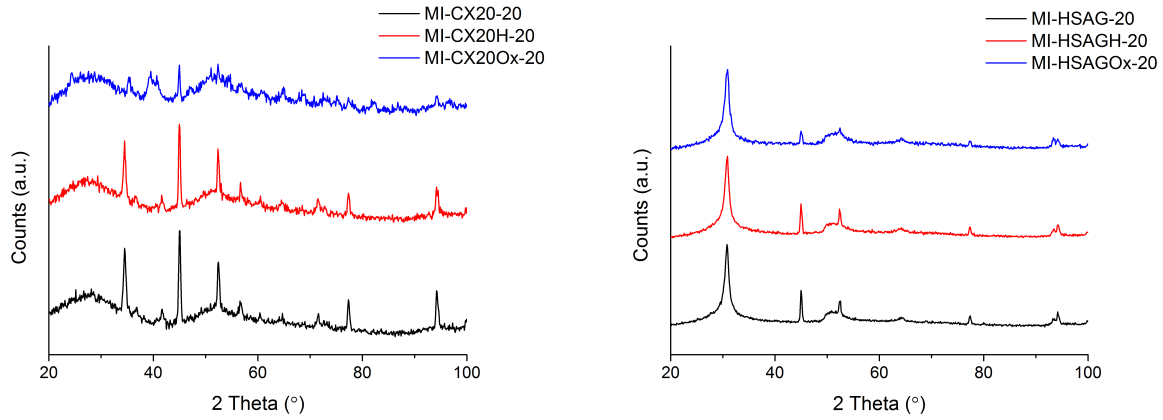

Figure 3.13 – *The XRD diffractograms show a cleaner melt infiltration for oxidized supports (less crystalline material). The reduced supports are identical to the pristine materials.*

gen. The catalysts with reduced supports on the other hand, release up to 25% more hydrogen and especially for the HSAG-H catalyst the onset and peak temperatures of release shifted to lower values.

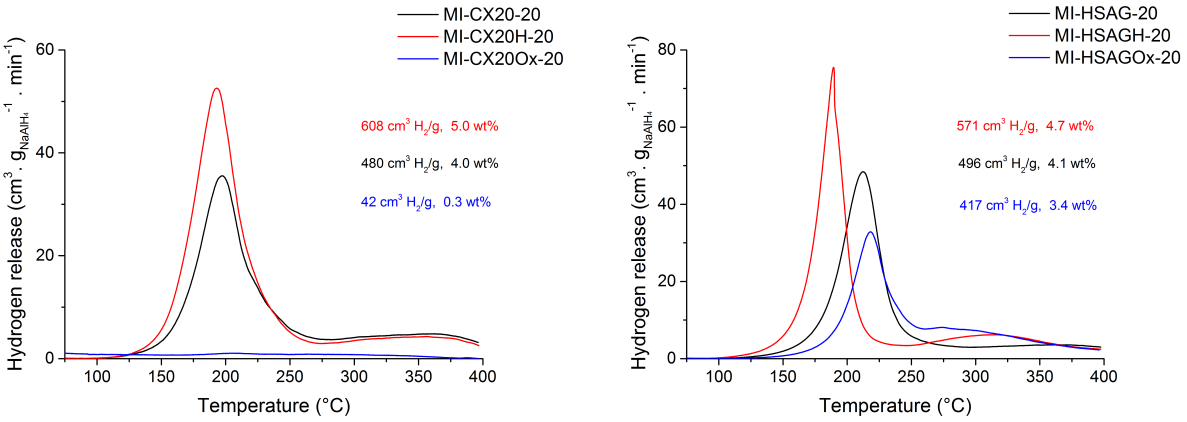

Figure 3.14 – *The TPD profiles lead to expect that the reduced supports will lead to more active catalysts, while the oxidized supports will be significantly less active.*

When combining these results with those of catalytic testing in the conversion of DPA, (Figure 3.15) some surprising conclusions can be drawn. The oxidized supports make for better catalysts than would be expected from the characterization, while the reduced supports do not live up to the expectations set by their TPD profiles. For both support materials, the pristine support needs the least amount of time to reach 50% DPA con-

version. With a continuous process in mind, this means the pristine supports would be most interesting. For batch processes, the CX-20-H supported catalyst would also be a good candidate, leading to higher DPA conversions after 24 hours of reaction time.

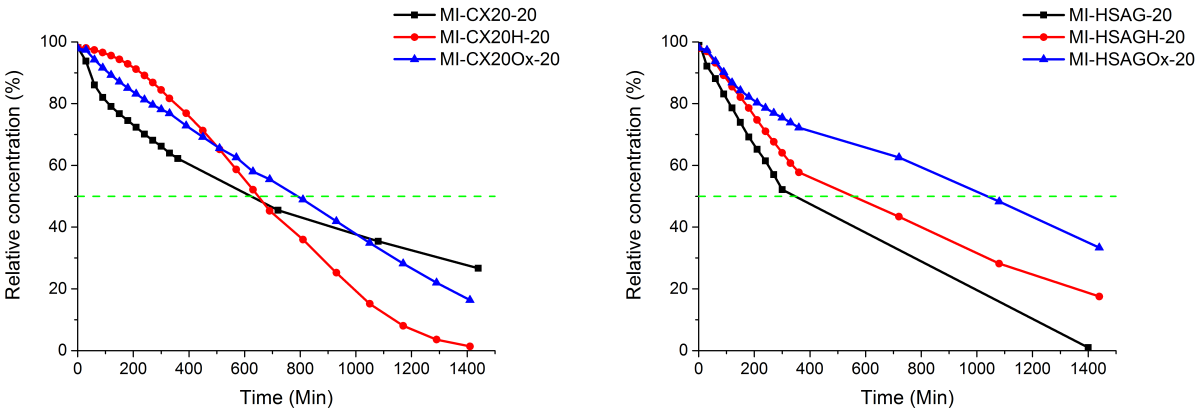

Figure 3.15 – *DPA conversions of differently supported catalysts. For clarity only the DPA depletion curves are shown. For both sets of supports, the pristine material outperforms the surface treated materials in the early stages of the reaction, up to at least 50% DPA conversion.*Conditions: *1 mmol $NaAlH_4$, 5 mmol DPA, 180 mL cyclohexane, 150 ˚C, 100 bar H_2.*

Even though the pristine supports used in this project seem to produce the best results, this does not mean the surface chemistry of the support can be ignored. Looking at the PSD and hydrogen release of differently treated supports, there can be expected to be a fine balance between surface chemistry and catalytic activity. This balance might involve, for example, the extent to which sodium alanate is oxidized, how strong it is bound to the anchoring sites on the support and how many discreet sodium alanate particles there are and their size. With the wide range of surface modifications that are possible using carbon as a support, more research will be needed to understand these effects more thoroughly.

3.2.4 Catalyst loading

To find the optimum sodium alanate to carbon weight ratio, four catalysts were prepared containing 5, 10, 20 and 40 wt% of sodium alanate. Nitrogen physisorption shows a strong decrease in pore volume from the original 0.831 cm^3/g of the support and indicates a higher degree of pore filling for higher sodium alanate weight loadings (Figure 3.16). The XRD diffractograms however, show an absence of crystalline sodium alanate for weight loadings up to 20%, but a significant amount of crystalline sodium alanate still seems to be present in the 40 wt% catalyst (Figure 3.17). The 40 wt%

catalyst can therefore be expected to be less active, since a significant amount of sodium alanate is not nanoconfined according to XRD, but according to physisorption, 75% of the pore volume is lost.

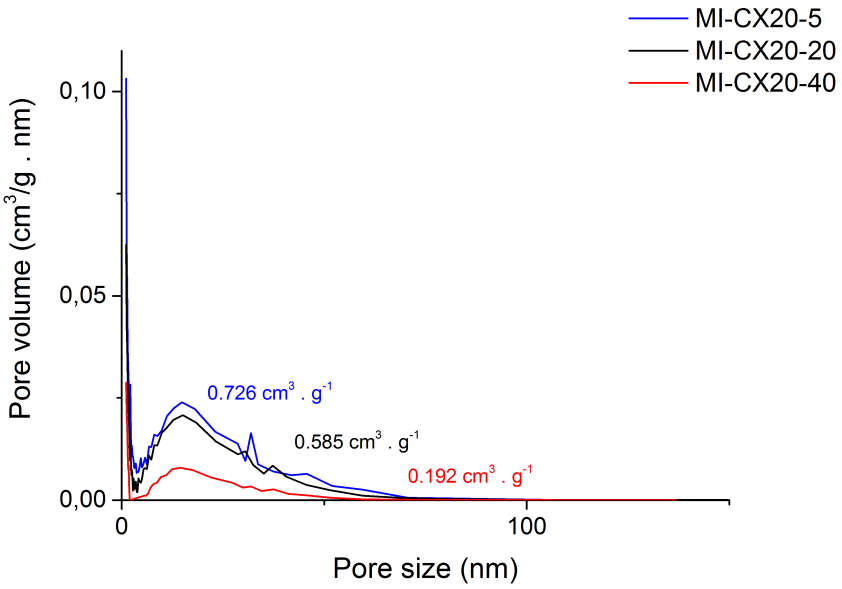

Figure 3.16 – *The nitrogen physisorption results for different weight loadings show more pore filling for higher loadings. However, the decrease in pore volume is larger than would be expected, probably because of pore blocking.*

The TPD profiles of the four catalysts with different weight loadings all have roughly the same peak onset around 100 °C and similar peak release temperatures (Figure 3.18). The 10 wt% catalyst unexpectedly releases more hydrogen than the 20 wt% catalyst, but in the previous sections it was shown that a higher amount of hydrogen released does not necessarily mean a catalyst is more active. Catalytic testing confirms this, as the 20 wt% catalyst clearly outperforms the other weight loadings, converting 50% of the DPA in 80 minutes, compared to $\sim$ 200 minutes for the other three loadings (Figure 3.19 and Table 3.5).

When normalizing the time it takes to reach 50% conversion to the amount of sodium alanate used, taking the 20 wt% catalyst as a baseline, the relative activities of the catalysts can be determined. The 5 wt% sodium alanate on CX-20 catalyst is the most active, needing 2.8 times as long to reach 50% conversion of DPA, but only needing 25% of the sodium alanate, making it $1/(2.8 * 0.25) = 1.4$ times as active (Table 3.5). The 40 wt% catalyst is clearly overloaded, with the double amount of sodium alanate causing a drop in total activity. The time needed to reach 50% conversion is increased by 2.5 times, meaning it performs on a similar level as the 5 wt% catalyst, while containing 4

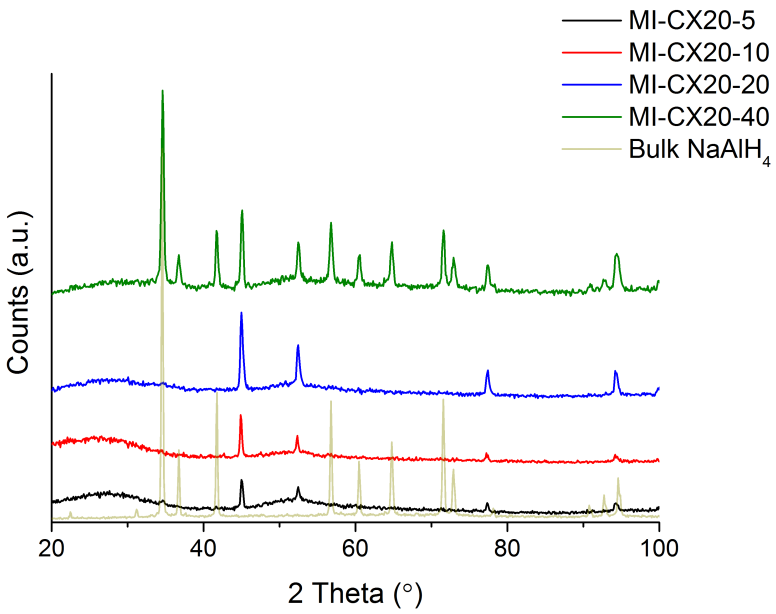

Figure 3.17 – *The XRD results for different catalyst loadings show a significant amount of crystalline sodium alanate remaining for the highest loading, meaning it did not enter the pores of the support. The other three catalysts do not show any sodium alanate peaks and can be expected to be more active, because all of the sodium alanate is nanoconfined.*

times as much sodium alanate. The 10 wt% catalyst seems to break with the trend that a lower weight loading gives a higher relative activity. It is not clear what causes this behaviour, but experimental error can not be excluded. Further research is needed to be able to learn more.

Two interesting weight loadings remain. In terms of activity per gram of catalyst, the 20 wt% catalyst is most interesting and this catalyst will be used for the remainder of this project. In terms of activity relative to the amount of sodium alanate, the 5 wt% catalyst performs best, which might be useful for future research: if ever scaling up for technical applications a lower weight loading is favourable since it will cut the material costs as well as storage and transportation costs.

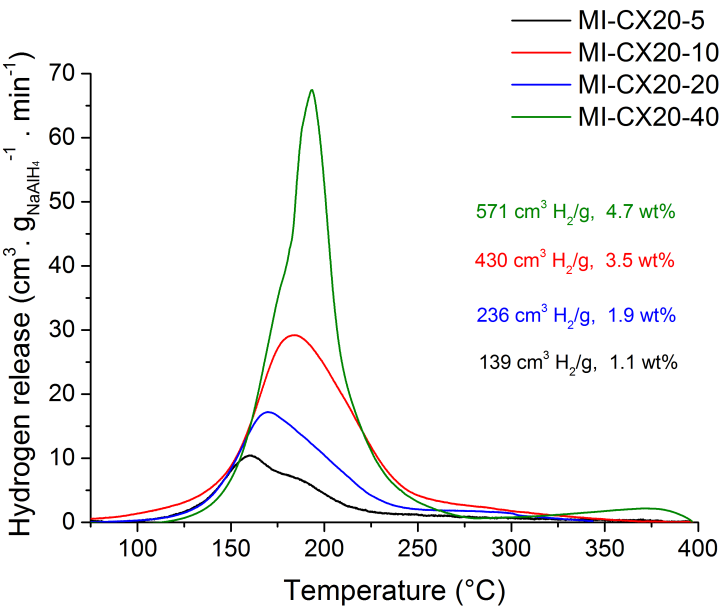

Figure 3.18 – *The TPD profiles of the catalysts containing different amounts of sodium alanate. Remarkably, the 10 wt% catalyst releases more hydrogen than the 20 wt% catalyst, but in previous experiments it turned out that a lower hydrogen release often resulted in higher catalytic activity.*

		Yield (%)		
Reaction	**Time to 50(%) conversion (min)**	**Cis**	**Trans**	**BB**
MI-CX20-5	225	29	4	17
MI-CX20-10	194	20	10	20
MI-CX20-20	80	9	31	8
MI-CX20-40	200	11	18	20

Table 3.5 – *Performance of catalysts containing different amounts of sodium alanate, in terms of time it takes to reach 50% conversion of DPA.*

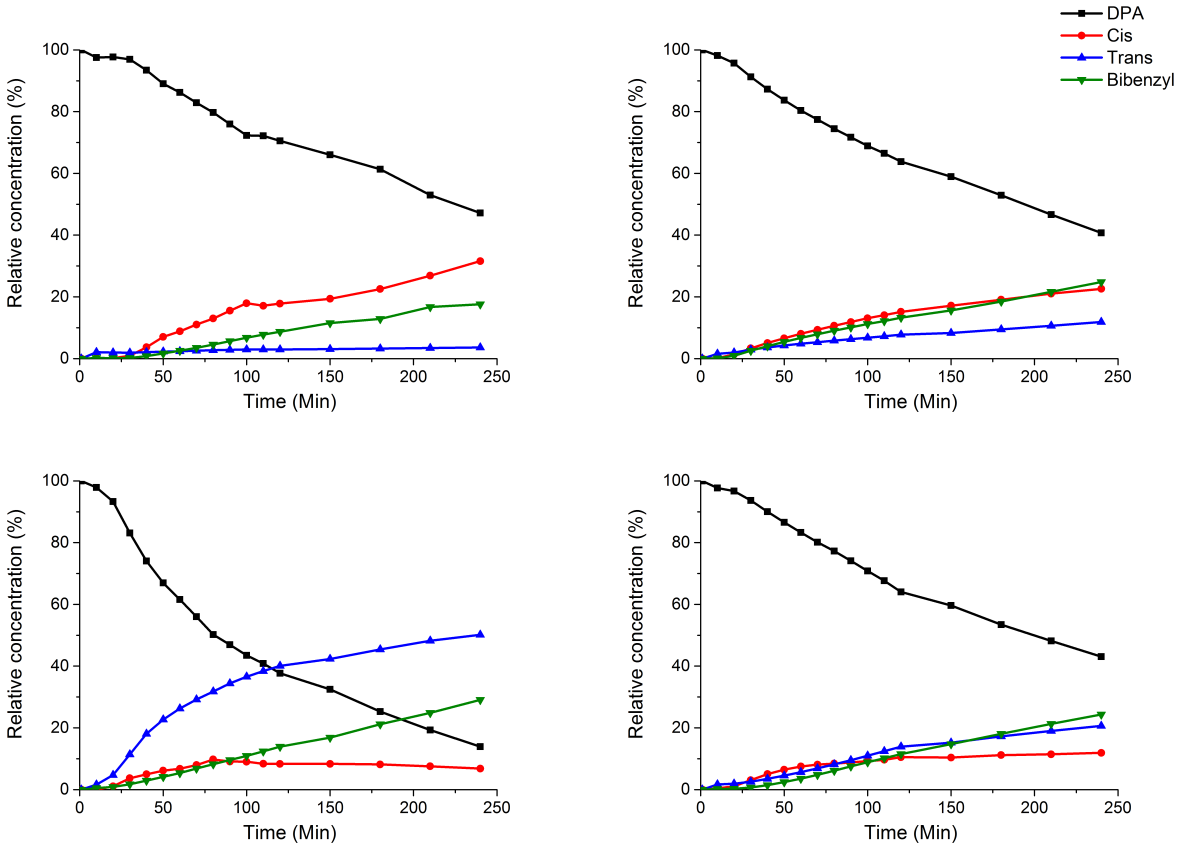

Figure 3.19 – Top left: *5 wt%.* Top right: *10 wt%.* Bottom left: *20 wt%.* Bottom right: *40 wt%.* Conditions: *1 mmol $NaAlH_4$, 5 mmol DPA, 180 mL cyclohexane, 190 ˚C, 100 bar H_2.*

Reaction	Normalized time to 50(%) conversion	Normalized loading	Relative activity
MI-CX20-5	2.8	0.25	1.4
MI-CX20-10	2.4	0.5	0.8
MI-CX20-20	1	1	1
MI-CX20-40	2.5	2	0.2

Table 3.6 – *Relative activity of catalysts containing different amounts of sodium alanate, normalized to the catalyst loading.*

3.3 Optimizing reaction temperature

Most reactions proceed faster when run at higher temperatures and a careful consideration has to be made between reaction the reaction speed and the reaction costs in terms of energy and equipment. Three reaction temperatures were investigated for catalysed hydrogenation over sodium alanate. When running the reaction at 100 °C, no catalytic activity was observed (Figure 3.20 as DPA conversion was similar to a blank reaction at 150 °C (Figure 3.21). At 150 °C however, the catalysed reaction converted 50% of the DPA in 300 minutes, indicating a minimum temperature for the catalyst to be active. By running the hydrogenation of DPA over nanoconfined sodium alanate at 190 °C instead of 150 °C the reaction speed was more than doubled, reaching 50 % conversion of DPA in 80 minutes instead of 300 (Figure 3.21). The reaction speed in a blank experiment at 190 °C also doubles, but a catalyst is still needed to rapidly convert DPA to bibenzyl. By running at higher temperature, the reaction time could be brought back to a more manageable 4 hours and this was used for any further experiments. The ideal balance between reaction time and reaction temperature depends on multiple factors, (e.g. the batch size, energy costs and limitations of equipment used) some of which are subject to change and therefore was not investigated any further.

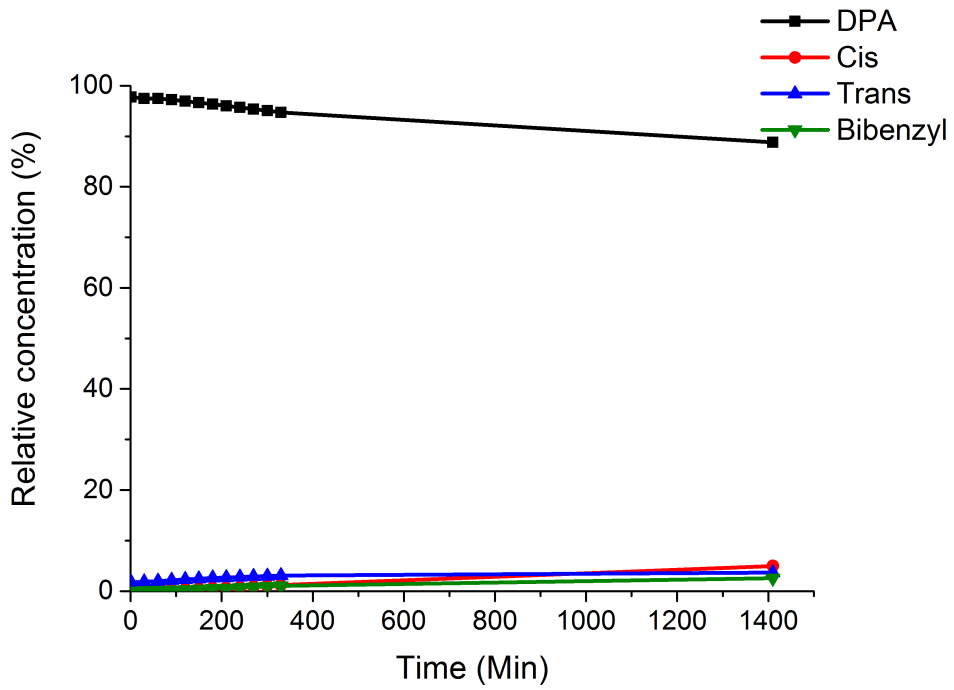

Figure 3.20 – *Results from reaction at 100 ˚C.* Conditions: *1 mmol $NaAlH_4$, 5 mmol DPA, 180 mL cyclohexane, 100 bar H_2.*

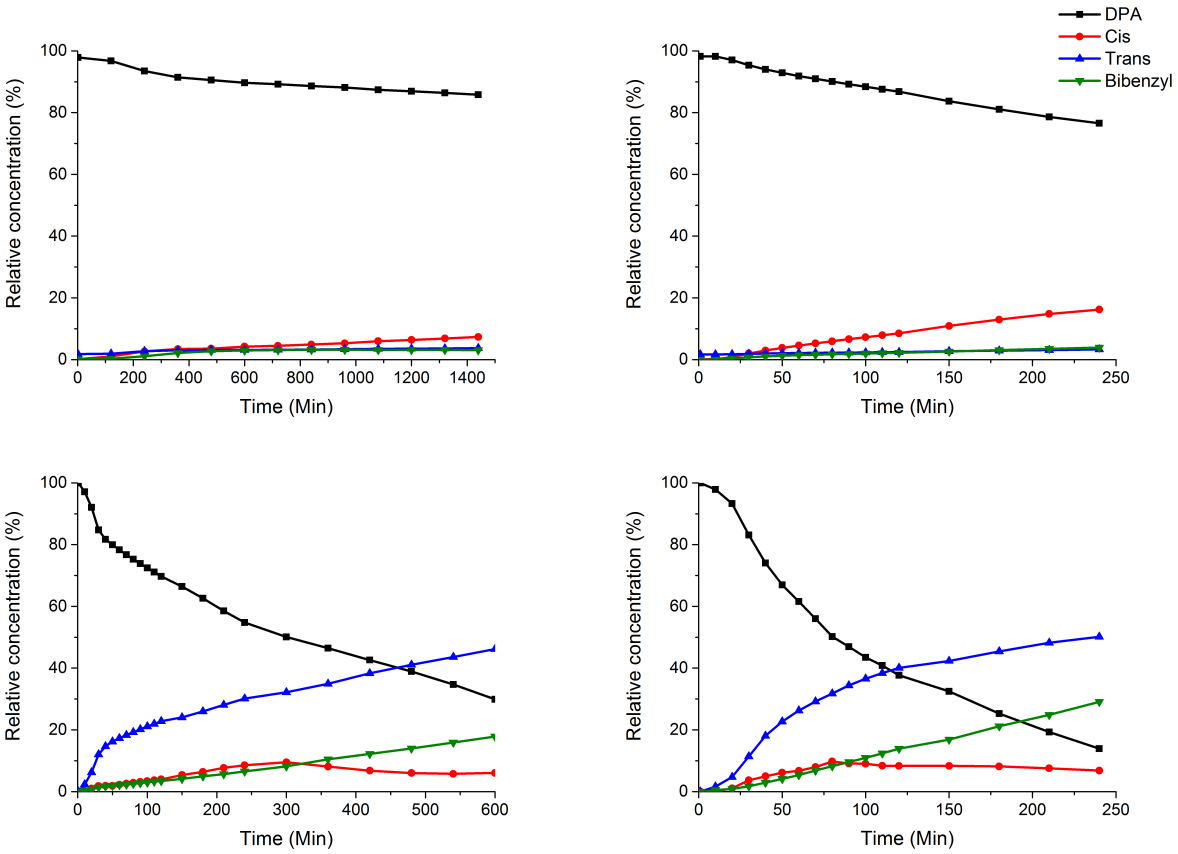

Figure 3.21 – *Results from blank (top) and catalyzed (bottom) reactions at 150 (left) and 190 (right) ˚C. Note that the timescales are different and the reactions at 190 ˚C proceed about twice as fast.* Conditions: *1 mmol $NaAlH_4$, 5 mmol DPA, 180 mL cyclohexane, 100 bar H_2.*

3.4 Best performing catalysts

After optimization of the catalyst preparation and reaction conditions, two catalysts (MI-CX20-20 and MI-HSAG-20) were tested to asses the improvement (Figure 3.22). Both support materials were tested, because the HSAG and CX-20 catalysts showed similar performance in previous tests. Both catalysts were characterized using N_2 physisorption, XRD and TPD and no significant differences could be found in comparison with previous catalysts. The full characterization of both catalysts can be found in the Appendix, but since no new observations were made compared to previous results they will not be discussed further.

In terms of performance the MI-CX20-20 and MI-HSAG-20 catalysts were very similar, both needing 80 minutes to reach 50% DPA conversion. After 4 hours, the DPA conversion is still equal with 87% of the DPA being hydrogenated, however, the MI-HSAG-20 catalyst produced more bibenzyl, giving a total yield of 42% against 30% for the MI-CX20-20 catalyst. This is probably caused by the HSAG catalyst either having a slightly higher turnover rate or a higher affinity for the conversion of the intermediate cis and trans products. The total turnover number, considering hydrogenation from a triple bond to a single bond as two reactions, was 5.76 and 6.44 for the CX-20 and HSAG catalysts respectively, assuming every molecule of sodium alanate to partake in the reaction. Since it is not yet clear what the active site looks like, it can not be said how much of the sodium alanate actually reacts and what the exact turnover number per active site would be. Since the HSAG has smaller pores than the CX-20 it can be expected that smaller sodium alanate particles give a slightly higher activity, but more tests are needed to confirm this, as the difference in activity can also be caused by the physical difference between HSAG and CX-20 (e.g. crystallinity, conductivity, etc.)

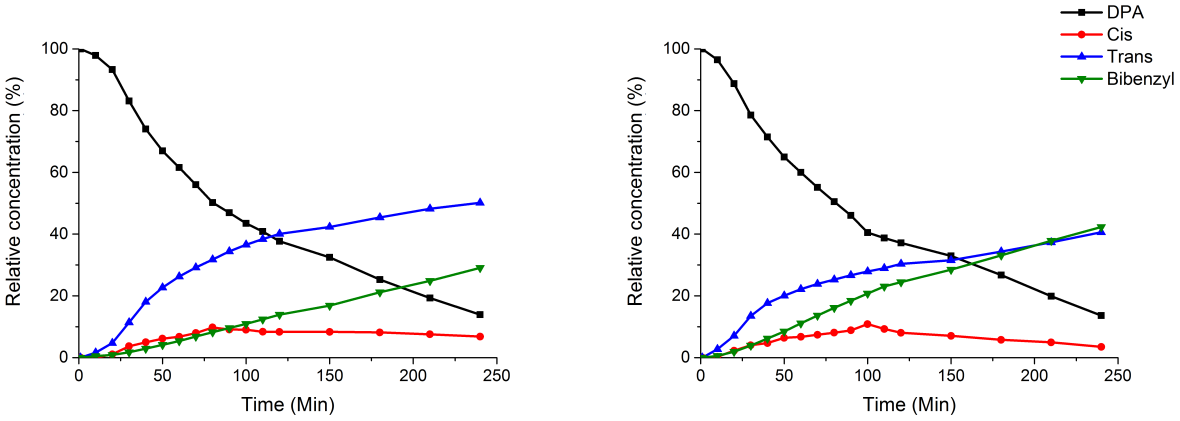

Figure 3.22 – *The best performing catalysts under the optimized conditions found in this project.* Left: *MI-CX20-20.* Right: *MI-HSAG-20.* Conditions: *1 mmol $NaAlH_4$, 5 mmol DPA, 180 mL cyclohexane, 190 ˚C, 100 bar H_2.*

3.5 Substrate screening

To see whether the nature of the bond that is to be hydrogenated influences the catalyst activity, a substrate screening was set up. four substrates were chosen with the molecular formula C_8H_{16}, but with different degrees of substitution on the double bond. The substrates were 1-octene (mono-substituted), 4-octene (di-substituted), 2,4,4-trimethyl-2-pentene (tri-substituted) and 2,3,4-trimethyl-2-pentene (tetra-substituted). By using substrates with the same molecular formula, it was attempted to eliminate as many variables as possible. The four substrates were tested in a reaction under the optimized conditions found for DPA, with the MI-HSAG-20 catalyst for a period of 3.5 hours at 190 °C. The reaction mixture was then measured with GCMS, to look at the composition (Figures 3.23, 3.24 and 3.25). The GC-MS results are qualitative results and can not be translated into exact concentrations.

A clear trend can be seen in the results. Where the reaction with 1-octene yielded mostly n-octane in a 2:1 ratio to the sum of the octene isomers that did not react, the reaction with 4-octene only showed half the conversion and for the tri- and tetra-substituted trimethylpentenes, no reaction was observed at all. This leads to the conclusion that double bonds with a lower degree of substitution are more readily hydrogenated by nanoconfined sodium alanate on carbon. The obvious explanation for this result is the steric hindrance induced by higher degrees of substitution, but experiments with different substituents on similar double bonds will have to be done to confirm this.

To test whether the catalyst would be able to hydrogenate carbonyl bonds and molecules containing oxygen atoms, two more substrates were tested using the same conditions as for the C_8H_{16} substrates. Trans-chalcone contains both a carbonyl bond and an olefinic bond. The GCMS analysis (Figure 3.26) shows partial hydrogenation of the carbon-carbon double bond, but the carbonyl bond does not react, leading to expect that the oxygen group deactivates the catalyst. GCMS analysis of allyl methyl ether (Figure 3.27) containing a double bond with the same orientation relative to an ether group instead of a carbonyl group, confirmed this suspicion, as no reaction took place at all. Other heteroatoms and functional groups may yet be tested, but oxygen containing substrates seem to either inhibit or deactivate the catalyst. Possibly this is caused by oxidation of the sodium alanate.

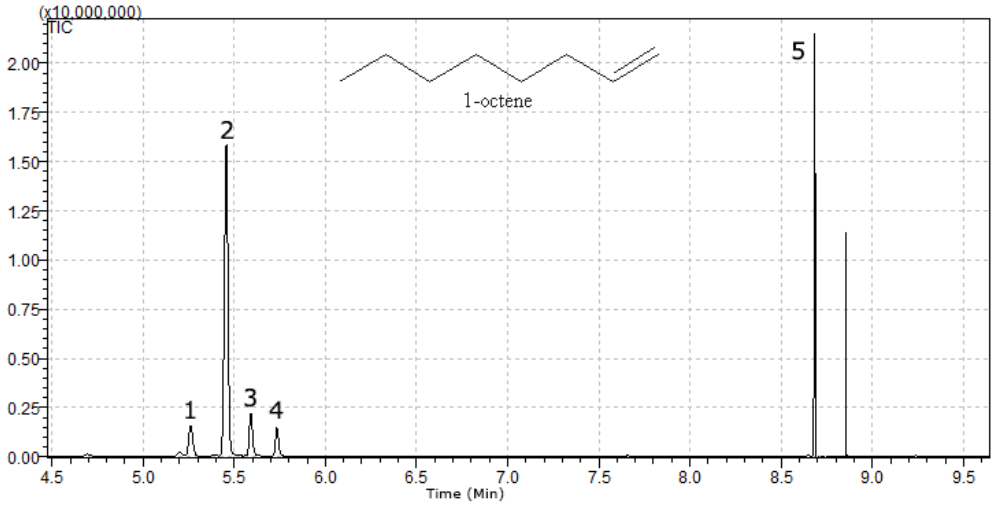

Figure 3.23 – *GCMS results of the hydrogenation reaction of 1-octene after 3.5 hours of reaction time. The peaks 1, 3 and 4 are caused by 1-, 2- and 4-octene. Peak 2 is the reaction product, n-octane and peak 5 is dodecane, which was used as an internal standard. A large amount of octene has been hydrogenated. The extra peak is not from the reaction mixture but from the inner lining of the GC-column.*

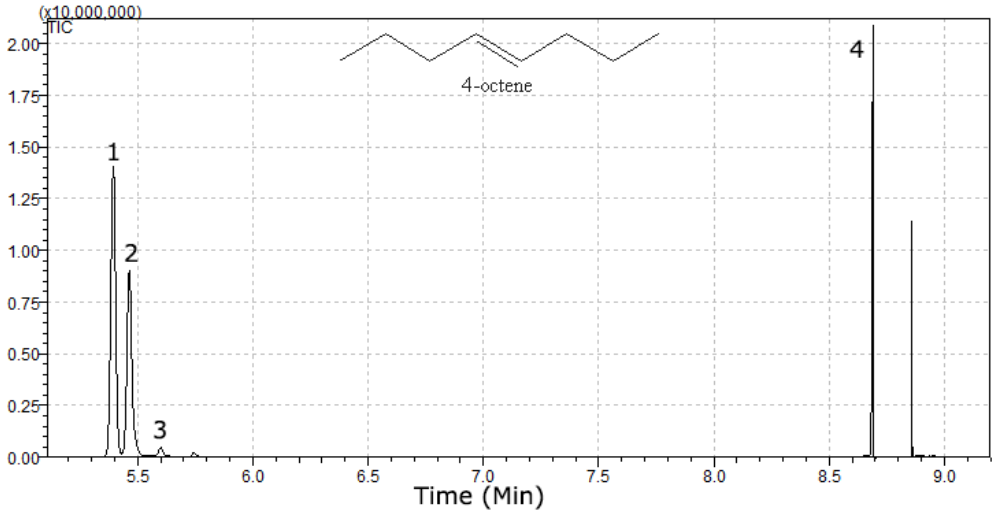

Figure 3.24 – *GCMS results of the hydrogenation reaction of 4-octene after 3.5 hours of reaction time. The peaks 1 and 3 are caused by 4- and 2-octene. Peak 2 is the reaction product, n-octane and peak 5 is dodecane, which was used as an internal standard. The extra peak is not from the reaction mixture but from the inner lining of the GC-column. While some of the 4-octene is hydrogenated, the yield is clearly worse than for the 1-octene.*

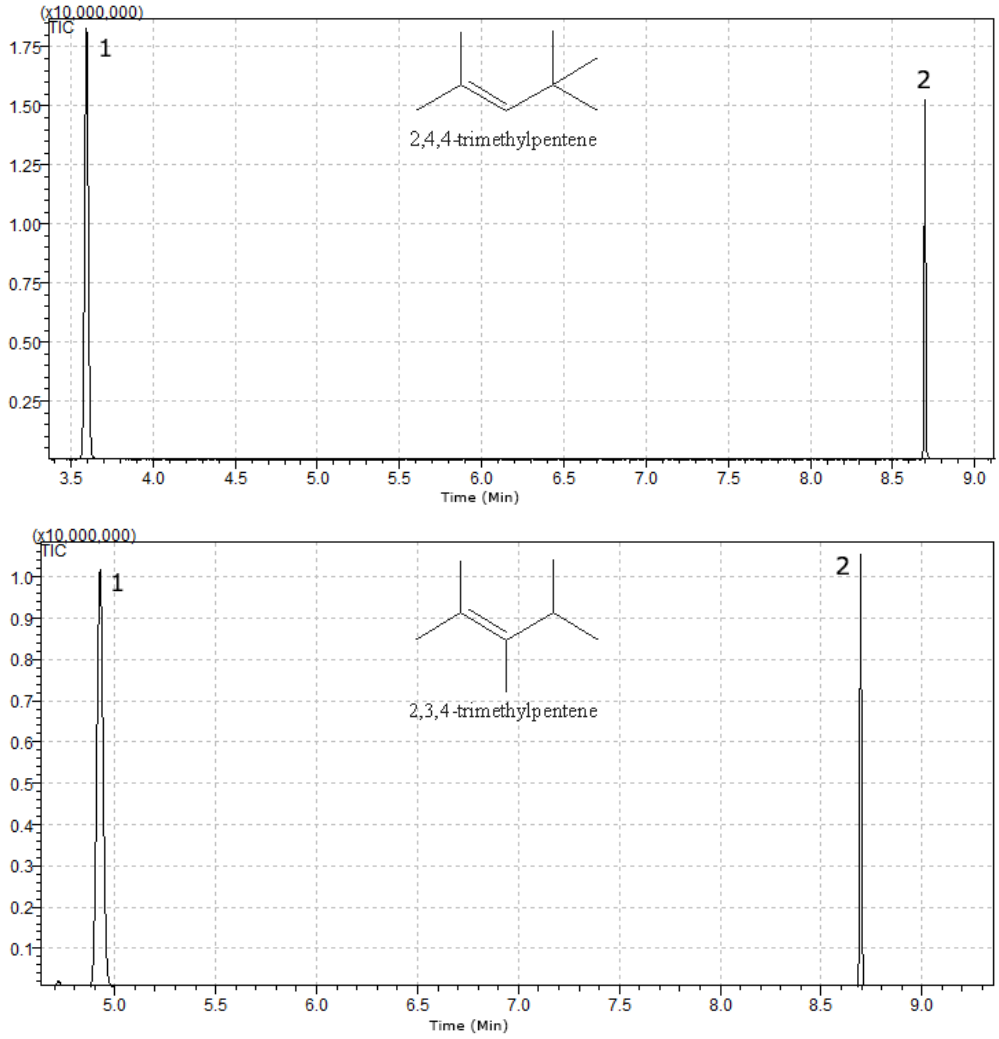

Figure 3.25 – *GCMS results of the hydrogenation reactions of 2,4,4-trimethylpentene (top) and 2,3,4-trimethylpentene (bottom) after 3.5 hours of reaction time. Both figures only show 2 peaks: that of the starting product (peak 1) and that of dodecane (peak 2). Both trimethylpentenes did not react at all.*

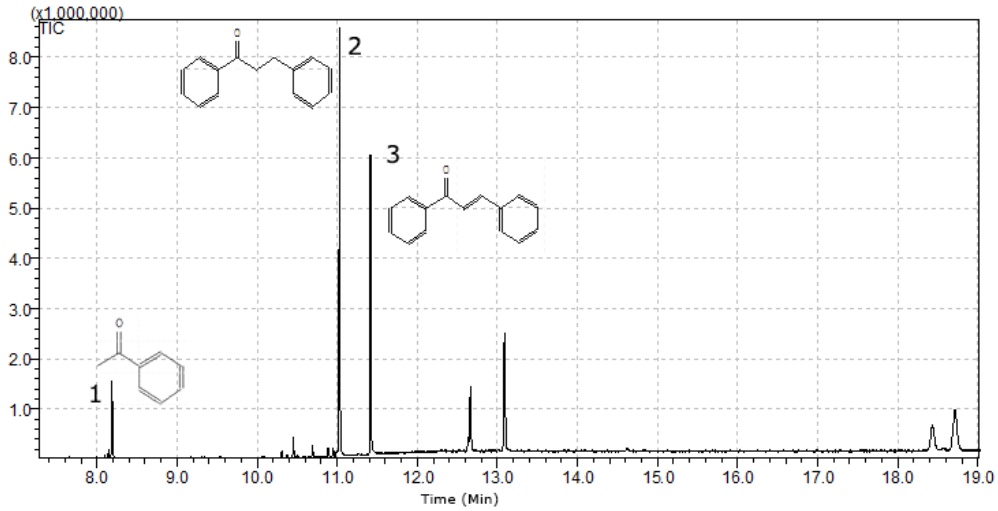

Figure 3.26 – *The GCMS results of the chalcone hydrogenation reaction. Peak one is an impurity from the substrate synthesis. Only the olefinic bond is partially (about two thirds) hydrogenated (peak 2), while the carbonyl bond did not react at all. Peak 3 is unreacted chalcone. The other peaks are from the column lining.*

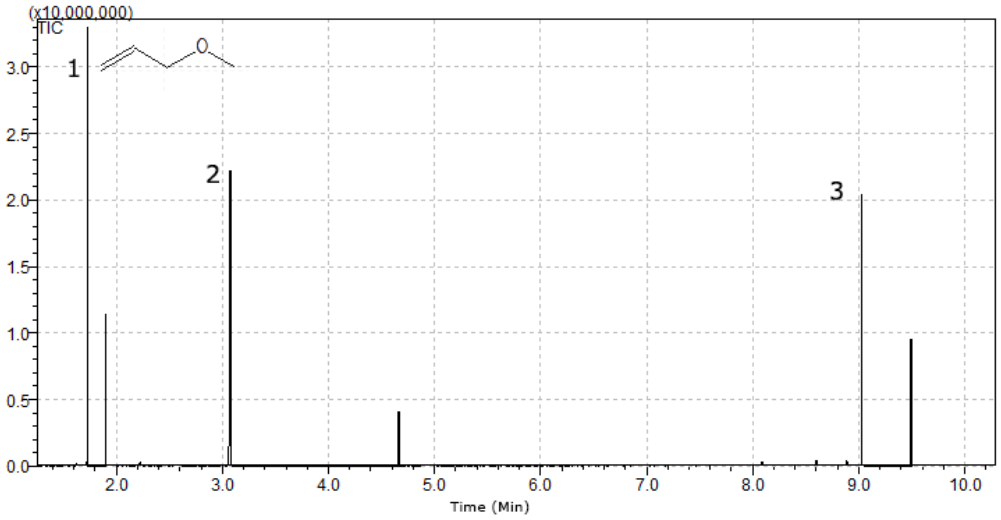

Figure 3.27 – *The GCMS results of the allyl methyl ether hydrogenation reaction. The first peak is the unreacted ether. The peaks 2 and 3 are cyclohexane and dodecane respectively, both were present in the reaction mixture. The other peaks are caused by impurities.*

3.6 Mechanistic experiments

To learn more about the mechanism and stereochemistry of hydrogen addition, norbornylene was tested as a substrate. Norbornylene is a cyclohexene molecule with a bridge between C1 and C4, making it a rigid molecule. The double bond can be hydrogenated to yield norbornane. It was tested in the reaction to see whether it would be hydrogenated. This reaction was only to test the suitability of norbornylene as a mechanistic probe and it was found that norbornylene was readily hydrogenated to norbornane using the MI-HSAG-20 catalyst (Figure 3.29). This meant norbornylene could be used as a mechanistic probe and a deuterium catalyst had to be prepared for mechanistic experiments.

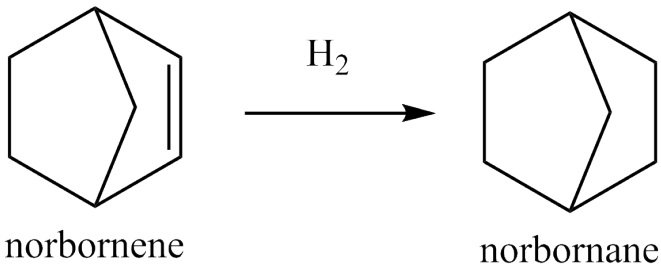

Figure 3.28 – *Norbornene (left) can be hydrogenated to yield norbornane (right).*

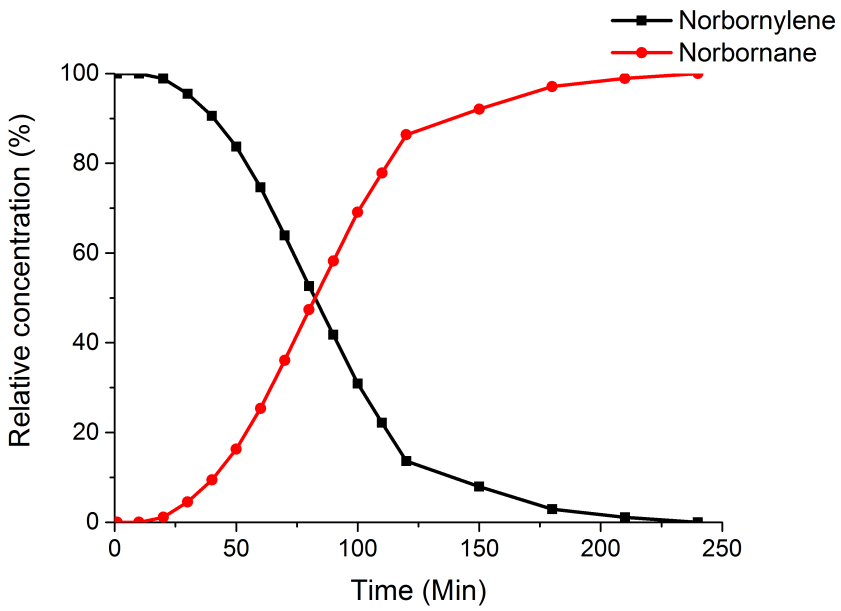

Figure 3.29 – *Hydrogenation reaction of norbornylene to norbornane.* Conditions: *1 mmol $NaAlH_4$, 5 mmol DPA, 180 mL cyclohexane, 190 °C, 100 bar H_2.*

3.6.1 Deuterated catalyst

By melt infiltration of sodium alanate on HSAG under deuterium atmosphere it was attempted to make a deuterated catalyst containing only $NaAlD_4$ as the active phase. To find out whether the preparation was successful, a TPD-MS experiment was done, where an MS scanning for hydrogen and deuterium gas was coupled to the TPD outlet (Figure 3.30). The normalized MS signals show a release of deuterium gas with the same profile as the release measured by TPD. A hydrogen signal is completely absent in the mass spectrum, leading to the conclusion that a deuterated sodium alanate catalyst was successfully prepared.

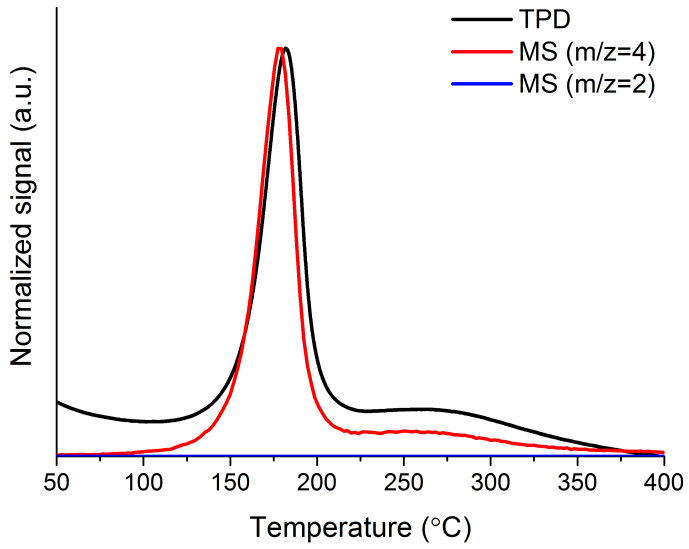

Figure 3.30 – *The TPD-MS measurement of the deuterated catalyst only shows deuterium release, which means al the hydrogen in the sodium alanate phase is replaced by deuterium. The measurement was done with a mass spectrometer coupled to the TPD setup, at a 5 ˚C per minute ramprate under argon flow.*

Additionally, a thermogravimetric analysis (TGA) experiment was run for the deuterated catalyst and the standard non-deuterated catalyst to compare it with (Figure 3.31). The deuterated catalyst shows a steep drop in mass of about 0.8 mg after reaching 120 °C under 45 bar of hydrogen pressure. With mass difference between the samples theoretically amounting to 1.3 mg due to the higher mass of deuterium, this change in mass can be explained by H/D exchange under the conditions mentioned. This means hydrogen release in the catalyst occurs for these conditions. This result can be related to the pilottemperature optimization experiments, where reaction at 100 °C did not show catalyst activity while reaction at 150 °C did. It also could mean that, when fully optimized for this catalyst, it should be possible to run a hydrogenation reaction at roughly 50 bar

of hydrogen pressure and a temperature upwards of 120 °C, even though the reaction will then probably be slower compared to the conditions used of 100 bar of hydrogen pressure and 190 °C.

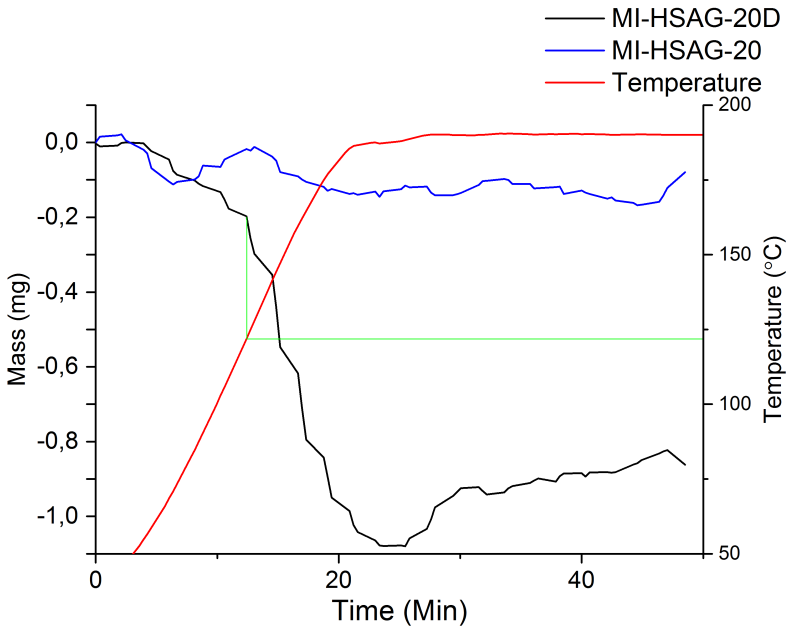

Figure 3.31 – *The TGA results of the deuterated and standard catalysts show H/D-exchange at 120 °C under 45 bar of hydrogen pressure.*

3.6.2 Deuterating norbornylene

Norbornylene was tested in a reaction using the deuterated sodium alanate catalyst and under deuterium atmosphere. This reaction could theoretically result in three products (Figure 3.32), which should be possible to differentiate between using NMR. This reaction was carried out in benzene, so there would be no interference with the cyclohexane signal in NMR.

According to literature, the norbornane NMR-spectrum looks as follows[37]:

1.0-1.3 ppm, 6H: multiplet of the 4 endo (pointing in the opposite direction as the bridge) protons on the carbons not participating in the bridge and the two protons on bridging carbon.

1.5 ppm, 4H: doublet with fine splitting of the exo (pointing in the same direction as the bridge) protons.

2.2 ppm, 2H: broad singlet of the protons on the bridgehead carbons.

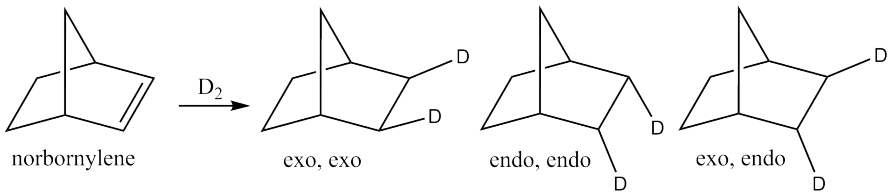

Figure 3.32 – *When deuterating norbornylene, three possible products could be formed. The absence of the trans product would indicate syn-addition and a concerted mechanism, whereas the presence of the trans product would indicate a stepwise reaction involving hydrides.*

Because the protons on different sides of the bond give different signals in the NMR spectrum, it should be possible to differentiate between products using a combination of ^{1}H and ^{2}H NMR.

First, a ^{1}H NMR spectrum was measured of pure norbornane to see whether the spectrum from literature could be reproduced (Figure 3.33, top). The measured spectrum resembled the literature and was then compared to the ^{2}H NMR spectrum of the reaction mixture supposedly containing deuterated norbornane (Figure 3.33, bottom). Only one peak can be seen which has the same chemical shift as the exo-protons of norbornane. This indicates the sodium alanate catalyst hydrogenates substrates in a syn-addition reaction. The selectivity to only the exo side leads to the conclusion that sterics play a role during the hydrogenation reaction and the sterically least congested reaction intermediate is formed. The absence of trans-deuterated products also implies the reaction proceeds through a concerted mechanism.

To be certain deuterium was only present on the carbon atoms that participated in the double bond of norbornylene an attached proton test was (APT) was done. In this spectrum CH_2 groups give a positive signal, while CH and CHD groups will give negative signals. When comparing pure norbornane (Figure C.1, top) with the deuterated product (Figure C.1) it can be seen that the peak related to the carbons in the former double bond is reduced in intensity and shows a negative triplet caused by the deuterium splitting the signal. On the other carbon atoms, no deuterium is found and the signals that are not marked are from dodecane, which was added as an internal standard to follow the reaction. The APT spectrum of dodecane can be found in the Appendix C for reference. This means that indeed the double bond is selectively deuterated from one side in a syn-addition.

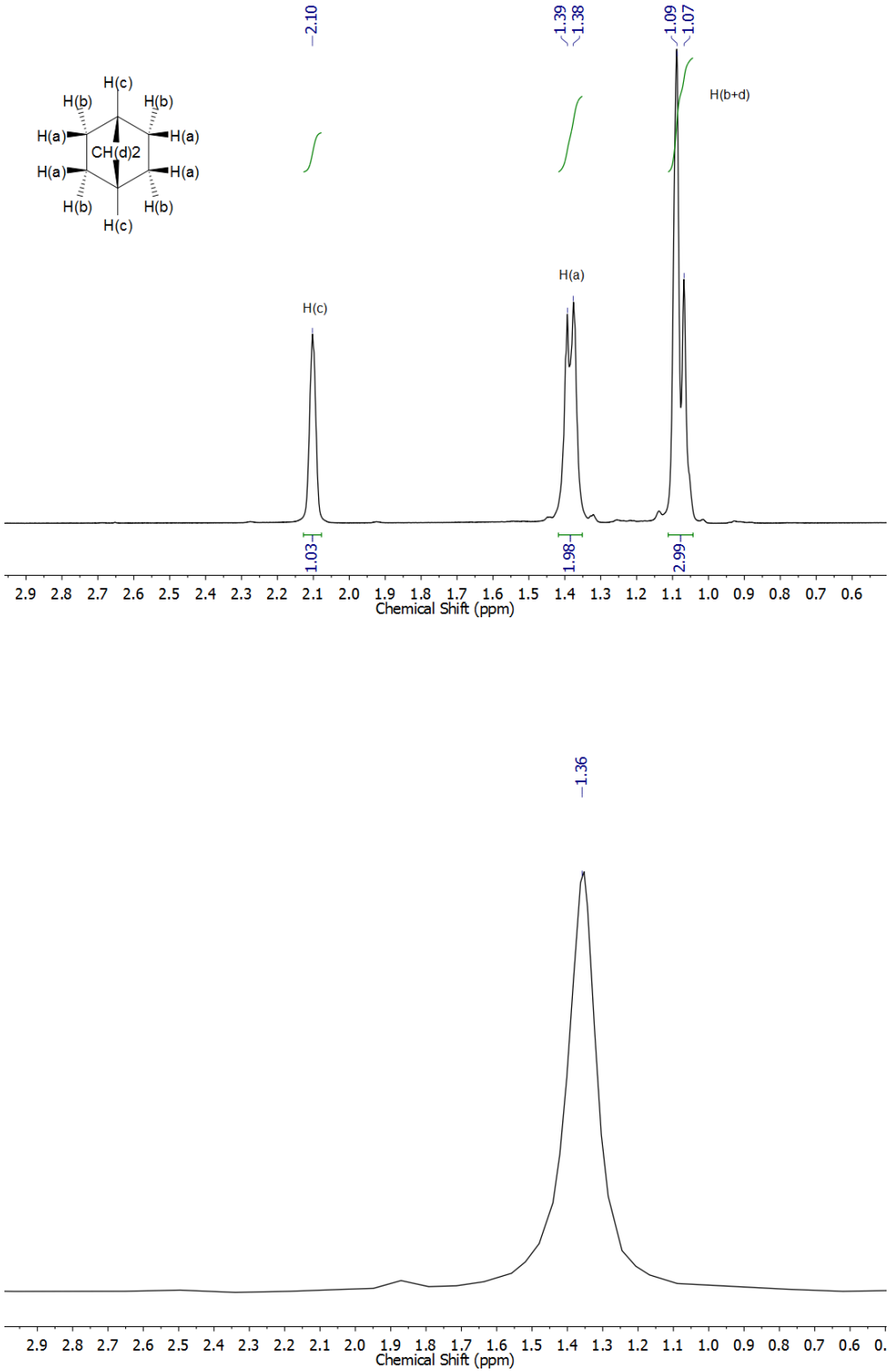

Figure 3.33 – *The ^{1}H NMR spectrum of pure norbornane (top) compared with the ^{2}H NMR spectrum of the deuterated reaction product (bottom). The samples were dissolved in benzene and deuterated benzene was added for the lock signal. The spectra were aquired on a 400 MHz machine. The position of the peaks show that deuterium is only incorporated on the exo position.*

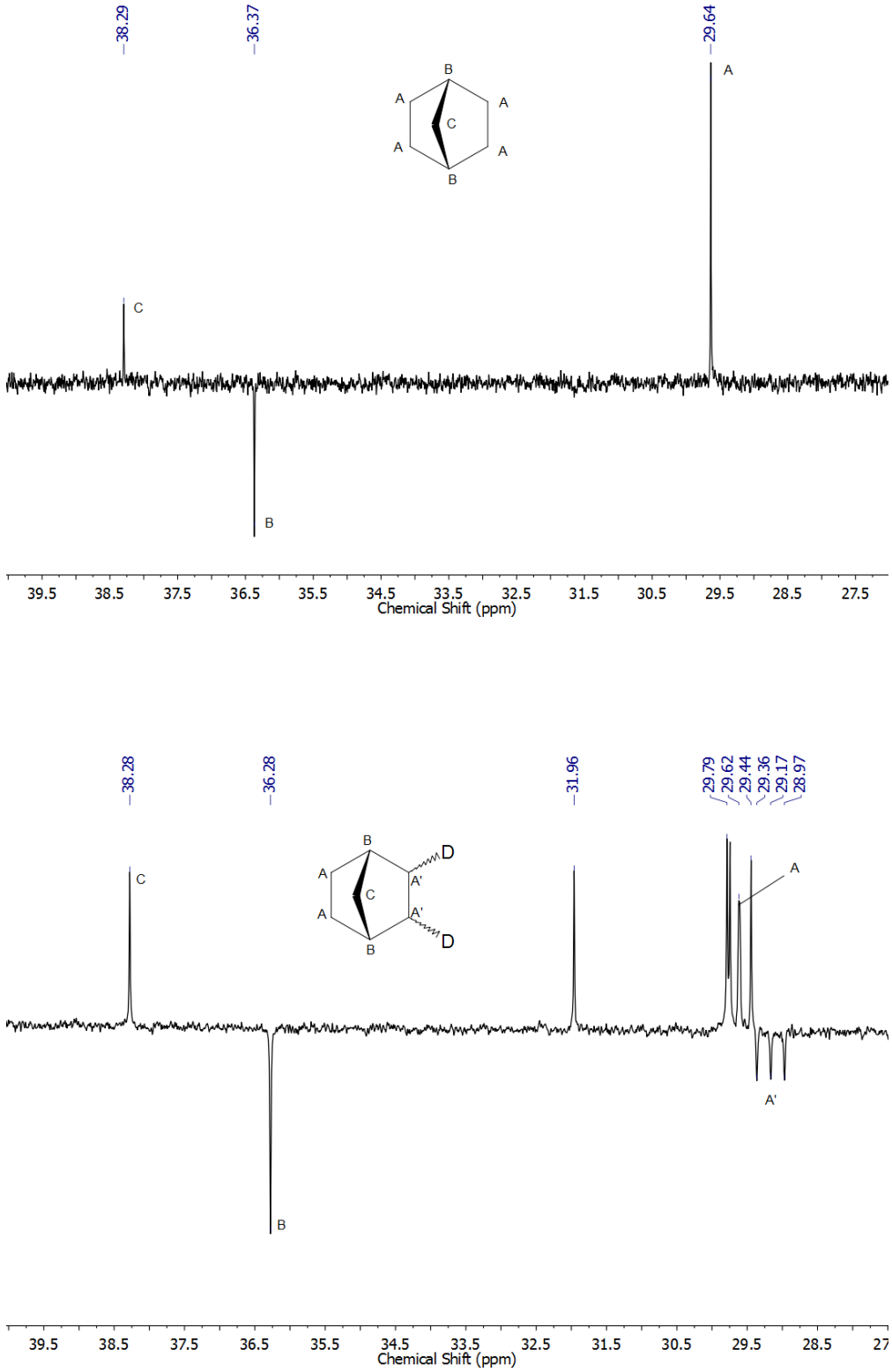

Figure 3.34 – *The APT spectra of pure norbornane (top) compared with the ^2H NMR spectrum of the deuterated reaction product (bottom) show that no deuterium is found on other carbon atoms, meaning the reaction was indeed a hydrogenation and not H/D-exchange. The samples were dissolved in benzene and deuterated benzene was added for the lock signal. The spectra were aquired on a 400 MHz machine.*

Chapter 4

Conclusion

This project has proven nanoconfined sodium alanate to be active as a hydrogenation catalyst in the hydrogenation of diphenylacetylene.

Nanoconfinement is essential for the catalyst to be active as was shown using an non-porous graphite support. Bulk sodium alanate does show hydrogen desorption yielding sodium and aluminium when heated to 200 °C, but regeneration of the catalytically active alanate phase is thermodynamically unfavourable. Nanoconfining sodium alanate at least partially addresses this problem, as can be seen from the stoichiometric ratio between catalyst and substrate: 1 mmol of nanoconfined sodium alanate can hydrogenate up to 10 mmol of double bonds.

Two different methods were used to prepare nanoconfined sodium alanate: Melt infiltration and incipient wetness impregnation. The catalysts prepared with incipient wetness impregnation were inferior to the melt infiltrated catalysts, which is expected to be caused by the THF solvent complexing to the sodium alanate. Diethylether was used in an attempt to replace THF, but dissolving sodium alanate in diethylether proved not to be possible.

To find out whether the support affects the catalytic activity catalysts were prepared on carbon xerogel and high surface area graphite supports. Initially the high surface area supported catalyst was twice as active as the catalyst prepared with carbon xerogel, but when the carbon xerogel was ground up before the melt infiltration the DPA conversion was similar. Surface treating the support materials under oxidative or reductive conditions yielded active catalysts, but the untreated supports outperformed the others in the region up to 50% DPA conversion.

Catalysts containing four different weight loadings of sodium alanate were prepared: 5, 10, 20 and 40 wt%. The 5 wt% catalyst showed the highest activity per equivalent of sodium alanate, while the 20 wt% catalyst showed the highest activity per time unit. 40 wt% of sodium alanate was overloading the support: the catalyst activity collapsed while it contained double the amount of sodium alanate compared to the most active catalysts.

By raising the reaction temperature from 150 °C to 190 °C it was possible to reach DPA conversions upwards of 90% in 4 hours instead of 24 hours. TGA experiments showed hydrogen desorption should occur at temperatures upwards of 120 °C, so a balance will have to be found between reaction temperature and reaction speed.

The best results were seen for the optimized catalysts, prepared by melt infiltration of 20 wt% sodium alanate with an untreated porous carbon support in a reaction at 190 °C under 100 bar H_2 pressure. Catalysts supported on carbon xerogel and high surface area graphite showed roughly the same DPA conversion, but HSAG supported catalyst produced significantly more bibenzyl. Assuming every sodium alanate molecule parttakes in the reaction, a turnover number of up to 6.44 double bond equivalents was reached in 4 hours time.

A nanoconfined sodium alanate catalyst can readily hydrogenate olefinic and acetylenic bonds, as long as they do not have sterically demanding substituents. This was demonstrated with diphenylacetylene (DPA) and a substrate screening containing double bonds with different degrees of substitution. Reaction with two oxygen containing substrates showed inactivity towards functional groups containing oxygen. For substrates containing both an oxygen group and an olefinic bond, the catalyst loses its activity, indicating either deactivation or inhibition by the oxygen containing groups.

It proved to be possible to make a deuterated form of the catalyst, where 100% of the gas released would be deuterium, by melt infiltrating under deuterium atmosphere without changing any of the other conditions. The deuterated catalyst was used in experiments to learn more about the catalytic mechanism. The catalyst turned out to hydrogenate norbornylene, yielding 100% of the cis,exo-deuterated product, which means the reaction proceeds through a concerted mechanism, performing syn-addition to the least sterically hindered side of a double bond.

Even though nanoconfined sodium alanate catalysts are not yet ready for industrial applications, they have been proven to work as a transition metal free hydrogenation catalyst. The initial results are promissing and if key problems like the harsh reaction conditions and the sensitivity of sodium alanate towards water and oxygen can be addressed, it might be interesting in future research and the development of a new class of catalysts.

Chapter 5

Outlook & Reccomendations

The catalysts in this project showed that more research could be done toward the effect of the properties of the CX-20 support on the catalytic activity. Multiple catalysts were prepared using the same batch of CX-20 and sometimes the catalytic performance differed significantly without a clear reason as to why. Possible experiments would be to vary the pore size of CX-20 supports, for example to get a more HSAG-like PSD, to see whether the size of the pores and thus the sodium alanate particles influences activity. Alternatively, more carbon supports could be tested to try and find the optimal support.

The XRD diffractograms of the melt infiltrated catalysts invariably showed an aluminium diffraction pattern. It would be interesting to find out if this crystalline aluminium phase is beneficial or rather inhibitory to the catalytic activity. By adding sodium hydride (NaH) to the melt infiltration, it might be possible to minimize the amount of metallic aluminium in the catalyst, while by increasing the duration or cycle the melt infiltration the amount of aluminium could be increased. Careful characterization of the amount of metallic aluminium and the size of the particles in combination with catalytic testing could provide more information about the role of aluminium and chemistry of the catalytically active phase.

Some preliminary experiments were done characterizing the catalyst using DSC and SEM, which might provide more detailed insights if continued. DSC experiments could tell something about phase changes taking place in the catalyst under reaction conditions , provided a DSC is used that can work under high enough hydrogen pressures. The problem that was encountered was decomposition of surface groups, giving undesirable signals and making analysis near impossible. This problem can be solved by using hydrogen treated support materials, minimizing the amount of surface groups that can interfere. Both the melt infiltration process and catalyst behaviour under reaction conditions could be looked at using this technique.

SEM and in particular SEM-EDX is a powerful way to look at the catalyst surface. Assuming that the chemistry takes place at the surface, surface mapping of both spent and fresh catalysts could tell something about the active catalytic phase and any possible change in the catalyst material during reaction. Some optimization might be needed, however, since the sodium alanate particles are in the nanometre scale and EDX mapping of elements with relatively close atomic weights could prove problematic.

Finally, there was a lack of time to test catalyst cycling. It would be interesting to see whether, if the DPA is replenished after a reaction and it is ran over the same catalyst, the catalyst would still be as active or already partially deactivated. Additionally an experiment using the standard catalyst under deuterium atmosphere might give information on the amount of active sites by measuring how much hydrogenated product is formed before deuterated product starts forming. This experiment has already been attempted, but so far, the low concentrations are problematic and accurate results not yet within reach.

Bibliography

[1] Streukens, G. & Schüth, F. Catalytic hydrogenations of tolane and stilbene with Ti- and Ce-doped complex metal hydrides. *J. Alloys Compd.* **474**, 57–60 (2009).

[2] Rylander, P. N. *Catalytic Hydrogenation over Platinum Metals* (Academic Press, New York, 1967).

[3] Liu, R.-J. *et al.* Metal sintering mechanisms and regeneration of palladium/alumina hydrogenation catalysts. *Appl. Catal. A Gen.* **282**, 111–121 (2005).

[4] Stephan, D. W. *et al.* Metal-free catalytic hydrogenation of polar substrates by frustrated Lewis pairs. *Inorg. Chem.* **50**, 12338–48 (2011).

[5] Stephan, D. W. & Erker, G. Frustrated Lewis pairs: metal-free hydrogen activation and more. *Angew. Chem. Int. Ed. Engl.* **49**, 46–76 (2010).

[6] Zaluska, A., Zaluski, L. & Ström-Olsen, J. Sodium alanates for reversible hydrogen storage. *J. Alloys Compd.* **298**, 125–134 (2000).

[7] Zakharkin, L., Gavrilenko, V., Maslin, D. & Khorlina, I. The preparation of aldehydes by reduction of esters of carboxylic acids with sodium aluminum hydride. *Tetrahedron Lett.* **4**, 2087–2090 (1963).

[8] Gao, J. *Carbon Matrix Confined Sodium Alanate for Reversible Hydrogen Storage.* Ph.D. thesis, Utrecht University (2012).

[9] Atkins, P. W., Overton, T., Rourke, J. P., Weller, M. & Armstrong, F. A. *Shriver & Atkins' inorganic chemistry*, 640 (Oxford University Press, 2010), 5 edn.

[10] Gao, J. *et al.* Enhanced reversibility of H_2 sorption in nanoconfined complex metal hydrides by alkali metal addition. *J. Mater. Chem.* **22**, 13209 (2012).

[11] Li, Y. *et al.* De-/re-hydrogenation features of $NaAlH_4$ confined exclusively in nanopores. *Acta Mater.* **59**, 1829–1838 (2011).

[12] De Jongh, P. E. & Adelhelm, P. Nanosizing and nanoconfinement: New strategies towards meeting hydrogen storage goals. *ChemSusChem* **3**, 1332–1348 (2010).

[13] Fichtner, M. Nanoconfinement effects in energy storage materials. *Phys. Chem. Chem. Phys.* **13**, 21186 (2011).

[14] Gao, J. *et al.* Confinement of $NaAlH_4$ in Nanoporous Carbon: Impact on H_2 Release, Reversibility, and Thermodynamics. *J. Phys. Chem. C* **114**, 4675–4682 (2010).

[15] Verkuijlen, M. H. W. *et al.* Solid-State NMR Studies of the Local Structure of $NaAlH_4$ / C Nanocomposites at Different Stages of Hydrogen Desorption and Rehydrogenation. *Structure* **114**, 4683–4692 (2010).

[16] Bogdanović, B., Brand, R. a., Marjanović, A., Schwickardi, M. & Tölle, J. Metal-doped sodium aluminium hydrides as potential new hydrogen storage materials. *J. Alloys Compd.* **302**, 36–58 (2000).

[17] Araújo, C. M., Li, S., Ahuja, R. & Jena, P. Vacancy-mediated hydrogen desorption in $NaAlH_4$. *Phys. Rev. B* **72**, 165101 (2005).

[18] Zhang, J. L. & Wenqing. *Improvement on Hydrogen Storage Properties of Complex Metal Hydride* (InTech, 2012).

[19] Zaluski, L., Zaluska, a. & Ström-Olsen, J. Hydrogenation properties of complex alkali metal hydrides fabricated by mechano-chemical synthesis. *J. Alloys Compd.* **290**, 71–78 (1999).

[20] Pinkerton, F. E. Comparison of hydrogen cycling kinetics in $NaAlH_4$-carbon aerogel composites synthesized by melt infusion or ball milling. *J. Alloys Compd.* **509**, 8958–8964 (2011).

[21] Baldé, C. P., Hereijgers, B. P. C., Bitter, J. H. & de Jong, K. P. Sodium alanate nanoparticles–linking size to hydrogen storage properties. *J. Am. Chem. Soc.* **130**, 6761–6765 (2008).

[22] De Jongh, P. E. & Eggenhuisen, T. M. Melt infiltration: An emerging technique for the preparation of novel functional nanostructured materials. *Adv. Mater.* **25**, 6672–6690 (2013).

[23] Adelhelm, P. *et al.* Comprehensive study of melt infiltration for the synthesis of $NaAlH_4$/C nanocomposites. *Chem. Mater.* **22**, 2233–2238 (2010).

[24] Stephens, R. D., Gross, A. F., Van Atta, S. L., Vajo, J. J. & Pinkerton, F. E. The kinetic enhancement of hydrogen cycling in $NaAlH_4$ by melt infusion into nanoporous carbon aerogel. *Nanotechnology* **20**, 204018 (2009).

[25] Baldé, C. P. *Sodium Alanate Nanoparticles for Hydrogen Storage.* Ph.D. thesis, Utrecht University (2008).

[26] Zheng, S. *et al.* Hydrogen Storage Properties of Space-Confined $NaAlH_4$ Nanoparticles in Ordered Mesoporous Silica. *Chem. Mater.* **20**, 3954–3958 (2008).

[27] Wang, J. *Development of Metal Complex Hydrides as Reversible Hydrogen Storage Materials.* Ph.D. thesis, University of South Carolina (2007).

[28] Li, W.-C., Lu, A.-H., Weidenthaler, C. & Schüth, F. Hard-Templating Pathway To Create Mesoporous Magnesium Oxide. *Chem. Mater.* **16**, 5676–5681 (2004).

[29] Esther G. Calvo, J. A. M. & Arenillas, A. *Nanomaterials*, 187–224 (InTech, 2011).

[30] Meier, S. R., Korwin, M. L. & Merzbacher, C. I. Carbon aerogel: a new nonreflective material for the infrared. *Appl. Opt.* **39**, 3940–3944 (2000).

[31] Cuervo, M. R. *et al.* Modification of the adsorption properties of high surface area graphites by oxygen functional groups. *Carbon N. Y.* **46**, 2096–2106 (2008).

[32] Li, H.-Q., Wang, Y.-G., Wang, C.-X. & Xia, Y.-Y. A competitive candidate material for aqueous supercapacitors: High surface-area graphite. *J. Power Sources* **185**, 1557–1562 (2008).

[33] Auer, E., Freund, A., Pietsch, J. & Tacke, T. Carbons as supports for industrial precious metal catalysts. *Appl. Catal. A Gen.* **173**, 259–271 (1998).

[34] Díaz, E., Ordóñez, S., Bueres, R. F., Asedegbega-Nieto, E. & Sastre, H. High-surface area graphites as supports for hydrodechlorination catalysts: Tuning support surface chemistry for an optimal performance. *Appl. Catal. B Environ.* **99**, 181–190 (2010).

[35] Obbink, M. K. *Confinement Of MgH_2 Nanoparticles Within Carbon Aerogel.* Msc. thesis, Utrecht University (2012).

[36] Pekala, R. W. Organic aerogels from the polycondensation of resorcinol with formaldehyde. *J. Mater. Sci.* **24**, 3221–3227 (1989).

[37] Brown, H. C., Kawakami, J. H. & Liu, K.-T. Additions to bicyclic olefins. V. Effect of 7,7-dimethyl substituents on the stereochemistry and rates of cyclic additions to norbornenes (2002).

Appendix

A Full characterization of the optimized MI-CX20-20 catalyst

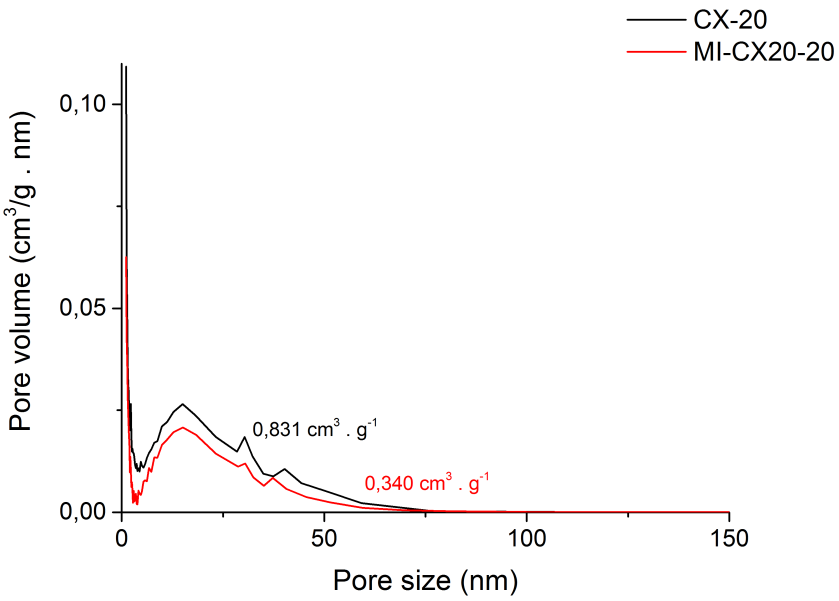

Figure A.1 – *Nitrogen physisorption of the best MI-CX20-20 catalyst.*

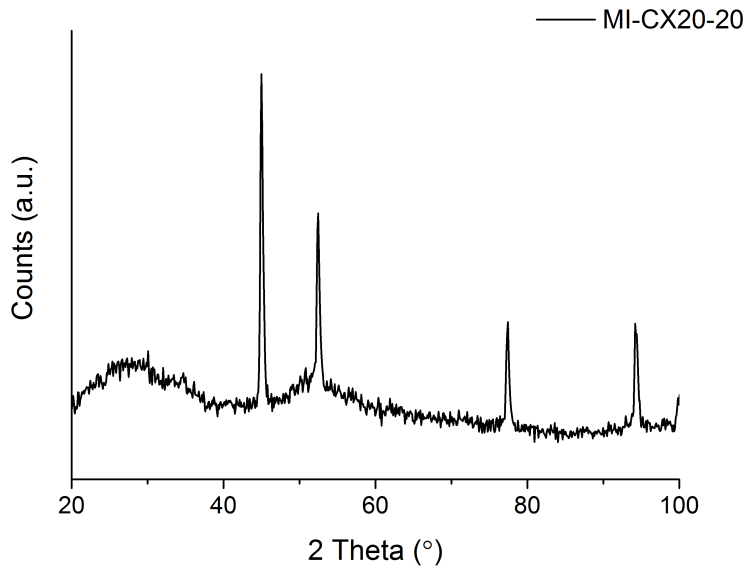

Figure A.2 – *XRD diffractogram of the best MI-CX20-20 catalyst.*

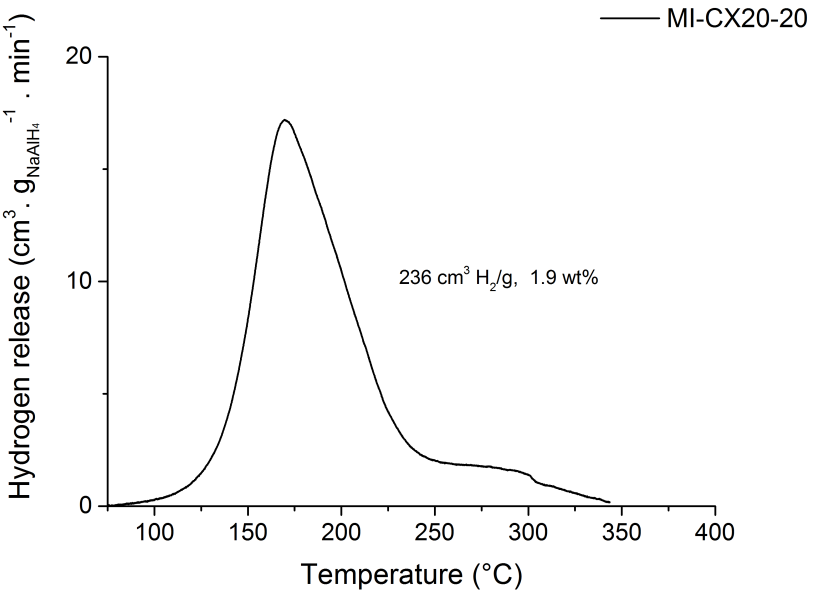

Figure A.3 – *TPD profile of the best MI-CX20-20 catalyst.*

B Full characterization of the optimized MI-HSAG-20 catalyst

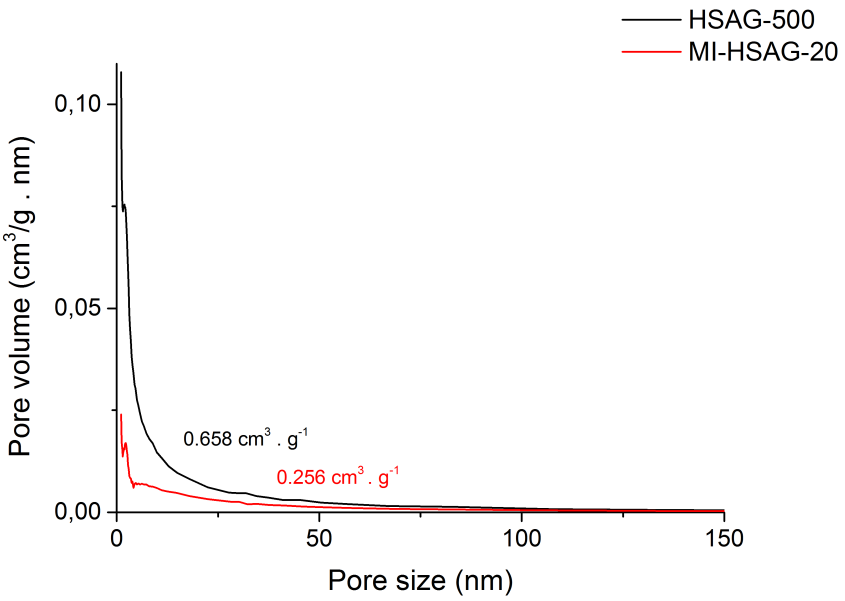

Figure B.1 – *Nitrogen physisorption of the best MI-HSAG-20 catalyst.*

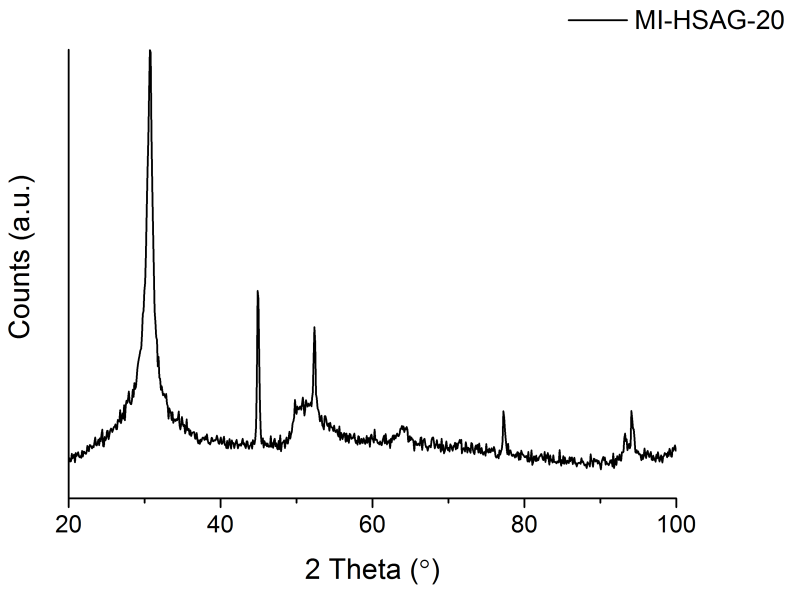

Figure B.2 – *XRD diffractogram of the best MI-HSAG-20 catalyst.*

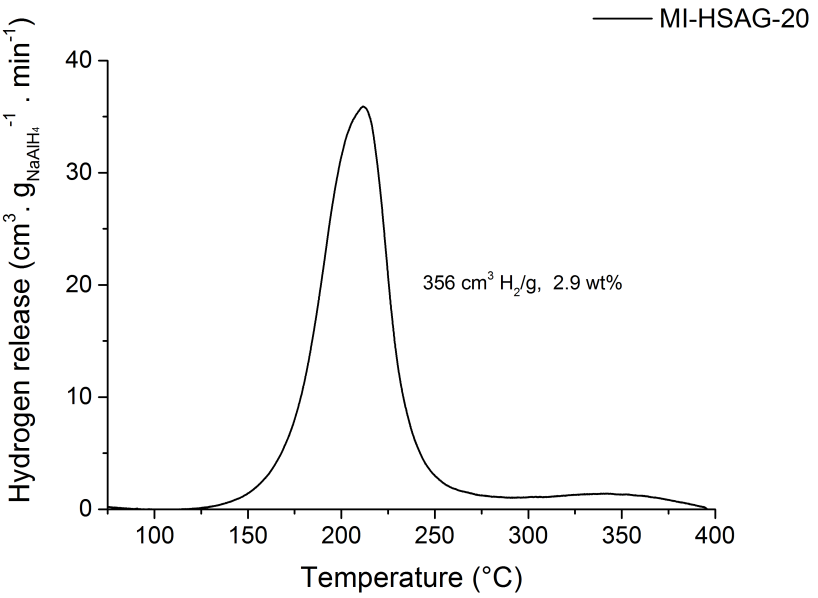

Figure B.3 – *TPD profile of the best MI-HSAG-20 catalyst.*

C APT NMR spectrum of dodecane

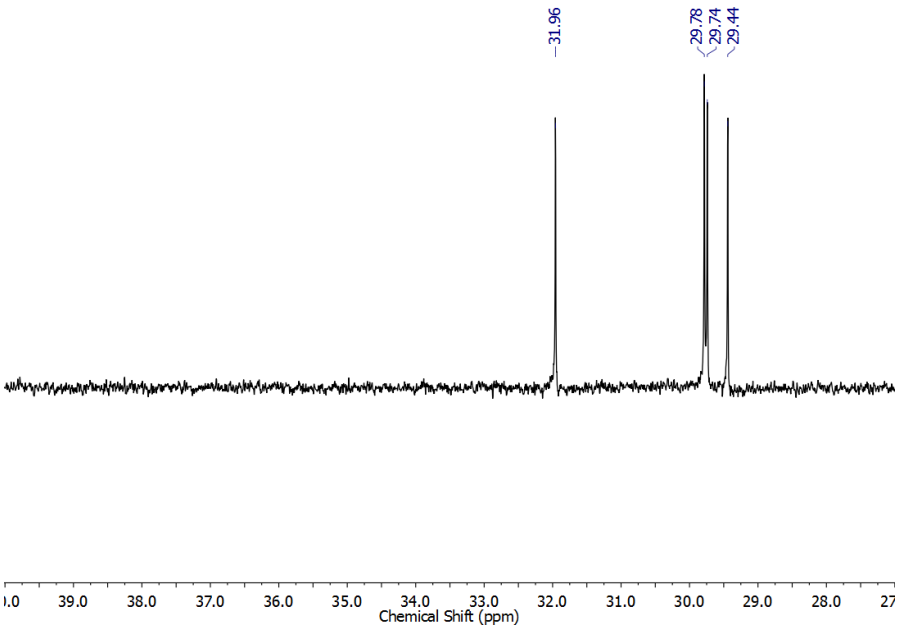

Figure C.1 – *APT spectrum for dodecane.*